Long-Term Performance of Epoxy-Coated Reinforcing Steel in Heavy Salt-Contaminated Concrete

U.S. Department of Transportation
Federal Highway Administration

FOREWORD

This report describes results obtained from a long-term natural weathering exposure testing of the remaining 31 post-Southern Exposure (SE) test slabs that contained epoxy-coated reinforcing bar (ECR), black bars, and stainless steel bars and were not autopsied during the 1993–1998 Federal Highway Administration (FHWA) research project. The test slabs had been exposed to the very aggressive SE test, which involved alternating wetting with 15 weight percent NaCl solution and air drying cycles for 96 weeks. The test results confirmed that the black bars produced the highest mean macrocell current density (least corrosion resistant) among various combinations of test variables regardless of slab configuration and the stainless steel bars exhibited negligible mean macrocell current density. The performance of straight top-mat ECRs varied from 7 to 40 percent of the highest black bar case, as measured by macrocell current density, depending on the size of the initial coating damage and the type of bar in the bottom mat. ECR used in the top mat alone reduced the corrosion susceptibility to at least 50 percent of the black bar case, even when it contained coating damage and was connected to the black bar bottom mat. If straight ECRs in the top mat were connected to ECRs in the bottom mat, the mean macrocell current density was no greater than two percent of the highest black bar case and approached the corrosion resistant level of stainless steel reinforcement. Autopsy of ECR slabs exhibiting negligible macrocell current density revealed excellent condition with no sign of corrosion. However, ECRs exhibiting high macrocell current densities showed coating deterioration and exhibited numerous hairline cracks and/or blisters in conjunction with reduced adhesion, coating disbondment (permanent loss of adhesion) and underlying steel corrosion. The test results of present and the earlier FHWA studies indicate that adhesion appeared to be a poor indicator of long-term performance of the coated bars in chloride contaminated concrete and it is concluded that there is no direct relationship between loss of adhesion and the effectiveness of ECR to mitigate corrosion.

This report will be of interest to materials and bridge engineers, reinforcing-concrete corrosion specialists, reinforcing bar manufactures, producers of organic coatings, and manufacturers of stainless steel.

T. Paul Teng, P.E.
Director, Office of Infrastructure
Research and Development

NOTICE

1. Report No. FHWA-HRT-04-090	2. Government Accession No.	3. Recipient's Catalog No.	
4. Title and Subtitle Long-Term Performance of Epoxy-Coated Reinforcing Steel in Heavy Salt-Contaminated Concrete		5. Report Date June 2004	
		6. Performing Organization Code	
7. Author(s) Seung-Kyoung Lee, Paul D. Krauss		8. Performing Organization Report No.	
9. Performing Organization Name and Address WISS, Janney, Elstner Associates, Inc. 330 Pfingsten Road Northbrook, IL 60062-2095		10. Work Unit No. (TRAIS)	
		11. Contract or Grant No. DTFH61-93-C-00027	
12. Sponsoring Agency Name and Address Office of Infrastructure R&D Federal Highway Administration 6300 Georgetown Pike McLean, VA 22101-2296		13. Type of Report and Period Covered Final Report September 1998 to December 2002	
		14. Sponsoring Agency Code	

15. Supplementary Notes
Contracting Officer's Technical Representative (COTR): Yash Paul Virmani, HRDI-10
Acknowledgements: Leo Zegler, John Drakeford, Gregory Hedien, Steve Harris, Steve Zimmerman

16. Abstract
This report describes long-term natural weathering exposure testing of the remaining 31 post-Southern Exposure (SE) test slabs that were not autopsied during the 1993–1998 Federal Highway Administration (FHWA) research project. The samples were exposed from September 1998 to December 2002 at an outdoor test yard in Northbrook, IL. The 1993–1998 research program involved testing more than 52 different bar materials and, consequently, 12 different bar types were selected for long-term durability tests in concrete exposed to the very aggressive SE test, which involved alternating wetting with 15 weight percent NaCl solution and drying cycles for 96 weeks. Periodic macrocell corrosion current between top and bottom mats and short-circuit potential data were collected during the exposure test program. Upon termination of the test program, autopsy and subsequent laboratory analysis was performed on the test slabs.

The test results confirmed that the black bars produced the highest mean macrocell current density (least corrosion resistant) among various combinations of test variables regardless of slab configuration, and that the stainless steel bars exhibited negligible mean macrocell current density. In general, bent epoxy-coated reinforcing bar (ECR) in the top mat, coupled with black bars in the bottom mat, performed the worst among all ECR cases. The straight top-mat ECRs' macrocell current density varied from 7 to 40 percent of the highest black bar case, depending on the size of initial coating damage and type of bar in the bottom mat. ECR used in the top mat alone reduced the corrosion susceptibility to at least 50 percent of the black bar case, even when it contained coating damage and was connected to the black bar bottom mat. In contrast, if straight ECRs in the top mat were connected to ECRs in the bottom mat, the mean macrocell current density was no greater than 2 percent of the highest black bar case even when rebar coatings had defects, and approach the corrosion resistant level of stainless steel reinforcement. Such improved corrosion resistance can be attributed to (1) reduction in cathodic area; (2) higher electrical resistance; and (3) reduced cathodic reaction.

Whenever an ECR slab with negligible macrocell current density was autopsied, the appearance of the extracted ECR and concrete/bar interface was excellent with no sign of corrosion. However, when ECRs specimens with high macrocell current densities were autopsied, they revealed coating deterioration due to corrosion and exhibited numerous hairline cracks and/or blisters in conjunction with reduced adhesion, coating disbondment (permanent adhesion loss), and underlying steel corrosion. No consistent trend was found between the level of macrocell current density and the extent of coating adhesion loss. The present test results and the earlier FHWA studies indicate that adhesion appeared to be a poor indicator of long-term performance of the coated bars in chloride contaminated concrete; it is concluded that there is no direct relationship between loss of adhesion and the effectiveness of ECR to mitigate corrosion.

Key Words concrete, corrosion, durability, electrochemical impedance spectroscopy, black bar, stainless steel, epoxy-coated reinforcing steel, mat-to-mat resistance, macrocell current, corrosion rate, chloride		18. Distribution Statement No restrictions. This document is available to the public through the National Information Service, Springfield, VA 22161.	
19. Security Classif. (of this report) Unclassified	20. Security Classif. (of this page) Unclassified	21. No. of Pages 130	22. Price

Form DOT F 1700.7   **(8-72)**   Reproduction of completed page authorized

SI* (MODERN METRIC) CONVERSION FACTORS

APPROXIMATE CONVERSIONS TO SI UNITS

Symbol	When You Know	Multiply By	To Find	Symbol
LENGTH				
in	inches	25.4	millimeters	mm
ft	feet	0.305	meters	m
yd	yards	0.914	meters	m
mi	miles	1.61	kilometers	km
AREA				
in^2	square inches	645.2	square millimeters	mm^2
ft^2	square feet	0.093	square meters	m^2
yd^2	square yard	0.836	square meters	m^2
ac	acres	0.405	hectares	ha
mi^2	square miles	2.59	square kilometers	km^2
VOLUME				
fl oz	fluid ounces	29.57	milliliters	mL
gal	gallons	3.785	liters	L
ft^3	cubic feet	0.028	cubic meters	m^3
yd^3	cubic yards	0.765	cubic meters	m^3
NOTE: volumes greater than 1000 L shall be shown in m^3				
MASS				
oz	ounces	28.35	grams	g
lb	pounds	0.454	kilograms	kg
T	short tons (2000 lb)	0.907	megagrams (or "metric ton")	Mg (or "t")
TEMPERATURE (exact degrees)				
^oF	Fahrenheit	5 (F-32)/9 or (F-32)/1.8	Celsius	^oC
ILLUMINATION				
fc	foot-candles	10.76	lux	lx
fl	foot-Lamberts	3.426	candela/m^2	cd/m^2
FORCE and PRESSURE or STRESS				
lbf	poundforce	4.45	newtons	N
lbf/in^2	poundforce per square inch	6.89	kilopascals	kPa

APPROXIMATE CONVERSIONS FROM SI UNITS

Symbol	When You Know	Multiply By	To Find	Symbol
LENGTH				
mm	millimeters	0.039	inches	in
m	meters	3.28	feet	ft
m	meters	1.09	yards	yd
km	kilometers	0.621	miles	mi
AREA				
mm^2	square millimeters	0.0016	square inches	in^2
m^2	square meters	10.764	square feet	ft^2
m^2	square meters	1.195	square yards	yd^2
ha	hectares	2.47	acres	ac
km^2	square kilometers	0.386	square miles	mi^2
VOLUME				
mL	milliliters	0.034	fluid ounces	fl oz
L	liters	0.264	gallons	gal
m^3	cubic meters	35.314	cubic feet	ft^3
m^3	cubic meters	1.307	cubic yards	yd^3
MASS				
g	grams	0.035	ounces	oz
kg	kilograms	2.202	pounds	lb
Mg (or "t")	megagrams (or "metric ton")	1.103	short tons (2000 lb)	T
TEMPERATURE (exact degrees)				
^oC	Celsius	1.8C+32	Fahrenheit	^oF
ILLUMINATION				
lx	lux	0.0929	foot-candles	fc
cd/m^2	candela/m^2	0.2919	foot-Lamberts	fl
FORCE and PRESSURE or STRESS				
N	newtons	0.225	poundforce	lbf
kPa	kilopascals	0.145	poundforce per square inch	lbf/in^2

*SI is the symbol for the International System of Units. Appropriate rounding should be made to comply with Section 4 of ASTM E380.
(Revised March 2003)

TABLE OF CONTENTS

LIST OF FIGURES

LIST OF TABLES

EXECUTIVE SUMMARY

In May 1993, the Federal Highway Administration (FHWA) began a 5-year research project, *Corrosion Resistant Reinforcing for Concrete Components*. The objective of the study was to develop cost-effective new breeds of organic, inorganic, ceramic, and metallic coatings, as well as metallic alloys that could be utilized on or as reinforcement for embedment in portland cement concrete and ensure a corrosion-free design life of 75 to 100 years when exposed to adverse environments. The 1993–1998 research program involved testing more than 52 different organic, inorganic, ceramic, and metallic coatings on steel bars, as well as solid metallic bars. Specifically, these included epoxy-coated, other polymer-coated, ceramic-coated, galvanized-clad, epoxy-coated galvanized-clad, stainless steel-clad, nickel-clad, copper-clad, corrosion resistance alloy-clad, inorganic silicate-clad, solid corrosion-resistance alloy steel, solid aluminum-bronze, solid stainless steels, and solid titanium reinforcing bars. Consequently, 12 different bar types were selected for long-term durability tests in concrete exposed to the very aggressive Southern Exposure (SE) testing, which involved alternating wetting with 15 weight percent NaCl solution and drying cycles for 96 weeks. About 150 test slabs were fabricated for the selected 12 different bar types.

After the conclusion of the 96-week SE testing in 1998, 31 post-SE test slabs that were not autopsied were then exposed to a long-term natural weathering at an outdoor test yard in Northbrook, IL, from September 1998 to December 2002. Periodic macrocell corrosion current between two mats and short-circuit potential of top mat bars (while they were connected to the bottom mat bars) data were collected during the exposure test program. When the test program ended after about 7 years, autopsy and subsequent laboratory analysis was performed with the test slabs, and the results are reported here. The tests include chlorides in the concrete, condition evaluation at bar/concrete interface, and visual examination of extracted bars.

Macrocell current density was a good indicator of corrosion performance of the various reinforcements. The black bars produced the highest mean macrocell current density (least corrosion resistant) among various combinations of test variables regardless of slab configuration. The stainless steel bars exhibited negligible mean macrocell current density. Whenever an epoxy-coated reinforcing bar (ECR) slab with negligible macrocell current density was autopsied, the appearance of the extracted ECR and concrete/bar interface was excellent with no sign of corrosion, and the coating looked new with a glossy texture. However, when ECRs slabs with a high macrocell current density were autopsied, they revealed coating deterioration due to corrosion and exhibited numerous hairline cracks and/or blisters in conjunction with reduction in adhesion, coating disbondment (permanent loss of adhesion), and underlying steel corrosion. Generally, the number of final coating defects on the autopsied ECRs increased from their initial values determined before embedment in concrete. There was no consistent trend found between the level of macrocell current density and the extent of coating adhesion loss. The earlier FHWA studies investigated the adhesion of the coatings using accelerated solution immersion tests and cathodic disbonding tests. Based on the review of the test results, the adhesion, as tested by solution immersion and cathodic disbonding tests, appeared to be a poor indicator of long-term performance of the coated bars in chloride contaminated concrete after 96-week SE. These findings led researchers to conclude that there is

no direct relationship between loss of adhesion and the effectiveness of ECR to mitigate corrosion.

In general, bent ECRs in the top mat coupled with black bars in the bottom mat performed the worst among all ECR cases. For straight top-mat ECRs, the mean macrocell current density was influenced by the size of initial coating damage and type of bar in the bottom mat. Their performance varied from 7 to 40 percent of the highest black bar case as measured by macrocell current density. However, if straight ECRs in the top mat were connected to ECRs in the bottom mat, the mean macrocell current density was no greater than 2 percent of the highest black bar case, regardless of the initial coating defect size. Both mat ECR systems behaved comparable to stainless steel bars. According to impedance modulus, alternating current (AC) resistance, macrocell current density data, and autopsy results, the excellent performance of test slabs containing ECRs in both mats should be attributed to the facts that electrical resistance was very high between the two mats, and the ECRs in the bottom mat suppressed the corrosion activity by minimizing the area for the cathodic reaction (oxygen reduction).

The 2-year saltwater ponding with alternate wetting, heating, and drying, followed by 5-year outdoor weathering, confirmed that use of ECRs in the top mat only (uncoated bottom mat) reduced the corrosion susceptibility to at least 50 percent of the black bar case, even when the coating has damage. Hence, ECR used in the top mat alone would not provide optimum corrosion protection. If ECRs are used in both mats in uncracked concrete, corrosion resistance increases dramatically, even when the rebar coatings have defects. Such improved corrosion resistance can be attributed to a (1) reduction in cathodic area; (2) higher electrical resistance; and (3) reduced cathodic reaction.

CHAPTER 1. INTRODUCTION AND PROJECT HISTORY

The Federal Highway Administration (FHWA) research project, *Corrosion Resistant Reinforcing for Concrete Components*, began in 1993. The objective of the proposed study was to develop cost-effective new breeds of organic, inorganic, ceramic, and metallic coatings, as well as metallic alloys that could be utilized on or as reinforcement for embedment in portland cement concrete. It was required that new coatings and alloys should provide significantly more corrosion-resistant reinforcement than the fusion-bonded epoxy-coated reinforcement that has been used in the United States since 1975 and also the corrosion-free design life shall be 75 to 100 years when exposed to adverse environments.

The research was aimed at developing new reinforcement materials and systems that minimally damage the coating system during (1) coating application, (2) fabrication bending operations, and (3) shipment to and installation at the jobsite. It was required that alloys have superior characteristics, and that thin-clad conventional steel resist damage. The coating systems had to have superior physical and chemical properties that remain undamaged by long-term exposure to ultraviolet radiation, high temperatures, salt-laden atmosphere, and other environmental conditions during long-term storage before casting them in concrete.

On March 3, 1993, 3M informed the researchers that Scotchkote 213 (3M 213™) would no longer be manufactured, because of rulings from the U.S. Environmental Protection Agency (EPA). The 3M 213 epoxy-coated bars had been used almost exclusively in the bridges in the United States from about 1980 to 1990. Based on this change, it became crucial to secure bars coated with the 3M 213 for the in-concrete tests that were to begin in 1995.

An invitational letter for submitting candidate bars was sent to 46 companies on May 17 and 18, 1993. It was anticipated that numerous new candidate organic coatings would be submitted for testing, because the 3M 213 epoxy coating material was no longer available, and new steel surface pretreatments used before coating the bars were being considered. As a result, researchers used a 30-day prescreening test program to screen these numerous organic-coated candidate bar systems, with and without special steel surface pretreatments. At that time, the organic coaters agreed that pretreatment would improve coating adhesion strength and long-term performance.

The 1993–1998 research program involved testing more than 52 different organic, inorganic, ceramic, and metallic coatings on steel bars, as well as solid metallic bars. Specifically, they included epoxy-coated, other polymer-coated, ceramic-coated, galvanized-clad, epoxy-coated galvanized-clad, stainless steel-clad, nickel-clad, copper-clad, corrosion resistance alloy-clad, inorganic silicate-clad, solid corrosion-resistance alloy steel, solid aluminum-bronze, solid stainless steels, and solid titanium reinforcing bars.

Prescreening tests on organic-coated bars were conducted from 1993 to 1995. These screening tests are chronicled in two reports: *The Performance of Bendable and Nonbendable Organic Coatings for Reinforcing Bars in Solution and Cathodic Disbondment Tests* [1] and the related phase II screening test report.[2] Screening tests were also conducted from 1993 to 1995 on

metallic-clad and solid metallic bars. This research studied 10 types of metal clad bars and 10 types of solid metal bars. The performance of various inorganic-, ceramic-, and metallic-clad bars and solid corrosion-resistant bars is discussed in the 1996 FHWA report, *The Corrosion Performance of Inorganic-, Ceramic-, and Metallic-Clad Reinforcing Bars and Solid Metallic Reinforcing Bars in Accelerated Screening Tests.*[3]

Based on screening tests as detailed in the three reports mentioned above, 12 bar types were selected for the 96-week in-concrete testing. The 141 reinforced concrete slab specimens using 12 different bar types were made and were exposed to the 96-week SE testing. These tests were completed in late 1997, and the final report was published in a 1998 FHWA report, *Corrosion Evaluation of Epoxy-Coated, Metallic-Clad and Solid Metallic Reinforcing Bars in Concrete.*[4]

The 96-week SE testing involved with the following wetting and drying cycles:

- Cyclic wetting and drying of 3-day drying at 38 ^{o}C (100 ^{o}F) and 60–80 percent relative humidity (RH), followed by 4-day ponding under a 15 percent NaCl solution at 16–27 ^{o}C (60–80 ^{o}F) for 12 weeks.
- Continuous ponding under a 15 percent NaCl solution at 16–27 ^{o}C (60–80 ^{o}F) and 60–80 percent RH for another 12 weeks.

The 15 percent salt solution was chosen to represent the high salt concentrations occurring on inland bridge structures from deicing salts. The long ponding period was utilized to simulate a sustained period of submersion or long periods of high concrete moisture common in winter months or in marine structures. This 24-week cycle was repeated four times for a total test period of 96 weeks.

Configuration of the concrete slabs used in this FHWA study measured 30.5 x 30.5 x 17.8 centimeters (cm) (12 x 12 x 7 inches) and contained two layers of 29.2-cm (11.5-inch) long and 1.6-cm (5/8-inch) diameter reinforcement, as shown in figure 1. The top mat acted as a macroanode and contained either two straight or two bent reinforcing bars, while the bottom mat was a macrocathode that contained four straight reinforcing bars. The top mat bar was connected to two bottom mat bars through a 10 Ω resistor. A clear cover of 25.4 millimeters (mm) (1.0 inch) was used in all specimens. This cover conforms to either the American Association of State Highway and Transportation Officials- (AASHTO) specified bottom-of-slab cover, or possible minimum in-place clear cover, allowing for construction tolerances when 3.8- to 5.0-cm (1.5- to 2.0-inch) cover requirements are specified. While most previous published corrosion studies used only crack-free concrete slabs, some of the test slabs used in this project contained the cracks directly over a top mat rebar to simulate cracks observed on actual bridge decks. Table 1 presents the concrete mix design data for the test slab concrete.
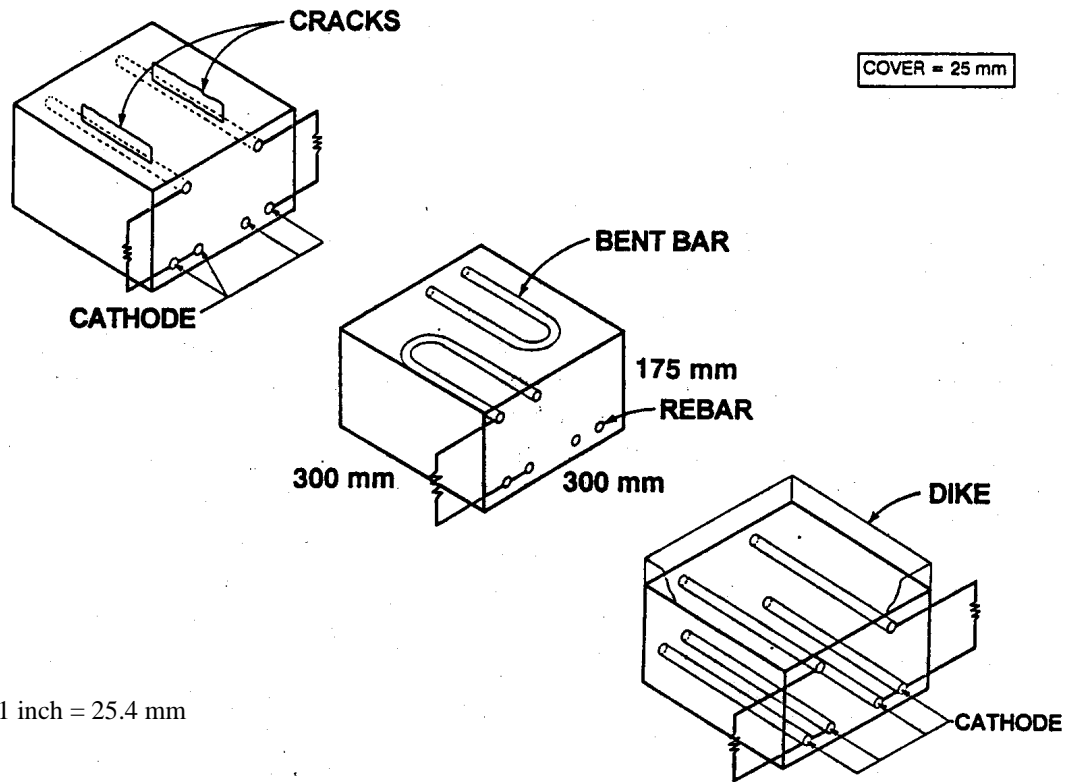
Figure 1. Configuration of test slab

Table 1. Mix properties of concrete used

Concrete Property	Mean Value of 30 Batches	Standard Deviation
Cement, kg/m^3 (lb/yd^3)	370 (623)	3.3 (5.56)
Air, percent	5.6	0.51
Slump, mm (inch)	167 (6.58)	31.7 (1.25)
Unit wt., kg/m^3 (lb/yd^3)	2315 (144.5)	21.0 (1.31)
w/c	0.47	0.01
28-day compressive strength, MPa (psi)	39.3 (5,700)	2.7 (403)

Table 2 shows the chloride concentration data collected during the 96-week FHWA study, and figure 2 shows the estimated chloride concentration at the top mat depth (2.5 cm or 1.0 inch) with time. It is clear that rapid migration of chloride is achieved through the SE testing. At the sixth week of testing, chloride concentration at the 2.5 cm (1.0 inch) depth exceeded 2.97 kg/m^3 (5 pounds (lb)/yard $(yd)^3$) (0.137 percent or 1,370 parts per million (ppm)), which was greater than 3 times the known chloride threshold (0.71 to 0.89 kg/m^3 (1.2 to1.5 lb/yd^3) or 300 to 350 ppm) for uncoated American Society for Testing and Materials (ASTM) A615 bar.

Table 2. Acid-soluble chloride concentrations (percent by weight of sample)

Test Period (Weeks)	Nominal Sampling Depth (inch)				Estimated Chloride at Top Mat	
	0.5	1.25	2.0	2.5	Percent by Weight of Sample	lb/yd^3
6	0.347	0.032	< 0.007	< 0.007	0.137	5.3
12	0.551	0.048	0.011	< 0.007	0.216	8.4
24	0.562	0.231	0.031	< 0.007	0.314	12.2
48	0.63	0.484	0.152	0.012	0.533	20.8
72	0.86	0.489	0.204	0.04	0.613	23.9
96	0.873	0.721	0.485	0.314	0.772	30.1

1 inch = 25.4 mm
1 lb/yd^3 = 0.59 kg/m^3
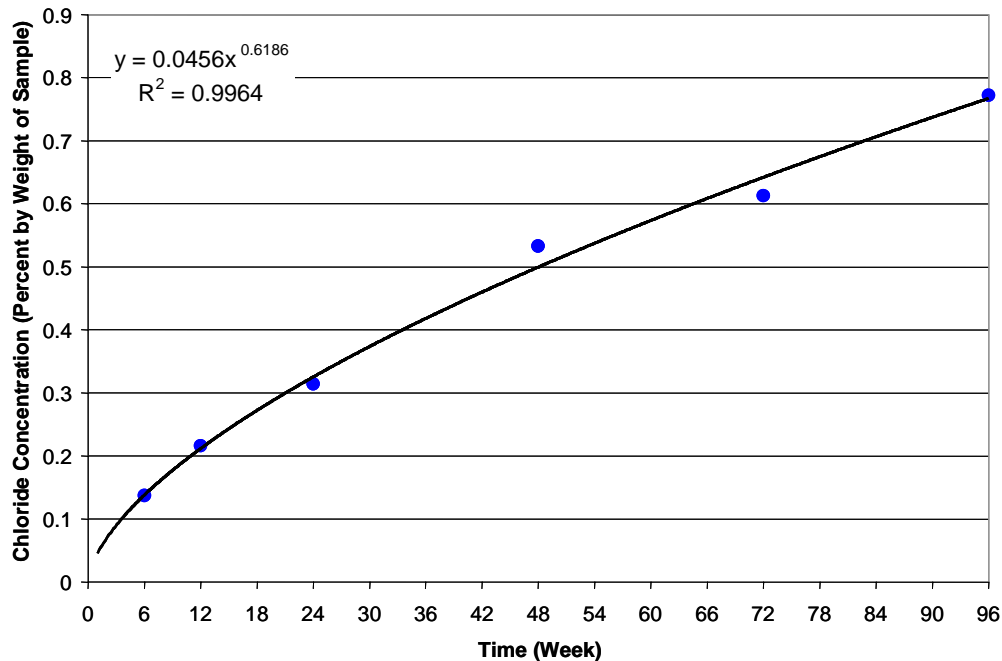
Figure 2. Estimated chloride accumulation at 25.4 mm (1.0 inch) depth with time in the concrete test slab

Table 3 summarizes the performance data of seven different rebar materials tested under the 96-week FHWA test program. Figures 3 and 4 show average macrocell current and mat-to-mat AC resistance data of each type reinforcing bar in table 3. Furthermore, table 4 classifies average macrocell current and mat-to-mat AC resistance of the ECR slabs for each coating type. The 96-week FHWA study concluded that the best ECR performance was obtained when the bars were tested in a straight condition, with 0.004 percent damage in uncracked concrete using an ECR cathode in the bottom mat. Researchers also found that there was a clear relationship between the mat-to-mat resistance values of the ECRs and their corrosion performance. Better corrosion protection was provided by those coating systems that had high electrical resistance, that is, the corrosion was strongly dependent on the amount of damage in the coating.[4]

Table 3. Summary of corrosion performance of different reinforcing bar materials under 96-week SE testing[4]

Bar Type	Slab Configuration	Macrocell Current		Mat-to-Mat Resistance		Slab Condition after 96 Weeks
		Average Macrocell Current over 96 Weeks (uA)	Percentage of Black Bar	Average AC Current over 96 Weeks (ohm)	Percentage of Black Bar	
ASTM A615 Black	Uncracked	352.5	100	243	100	All slabs cracked
	Precracked	405.3	100	263	100	
Six Different Epoxy-Coated Bar Types	Uncracked	0.2 to 190.7	0.06 to 54.1	704 to 659,069	290 to 271,222	Some slabs cracked or exhibited rust staining
	Precracked	1.4 to 191.8	0.35 to 47.3	591 to 103,722	225 to 39,438	
Galvanized Bar	Uncracked	207.9	59.0	413	170.0	All slabs cracked
	Precracked	294.1	72.5	318	120.9	
Zinc Alloy-Clad Bar	Uncracked	126.7	35.9	385	158.4	One slab cracked
	Precracked	273	67.3	325	123.6	Slabs cracked
Copper-Clad Bar	Uncracked	3.7	1.0	584	240.3	No damage observed
	Precracked	14.2	3.5	491	186.7	
304 Stainless Steel Bar	Uncracked	0.5	0.1	602	247.7	No damage observed
	Precracked	11.3	2.8	566	215.2	Minor staining on concrete surface
316 Stainless Steel Bar	Uncracked	0.5	0.1	476	195.9	No damage observed
	Precracked	0.5	0.1	429	163.1	
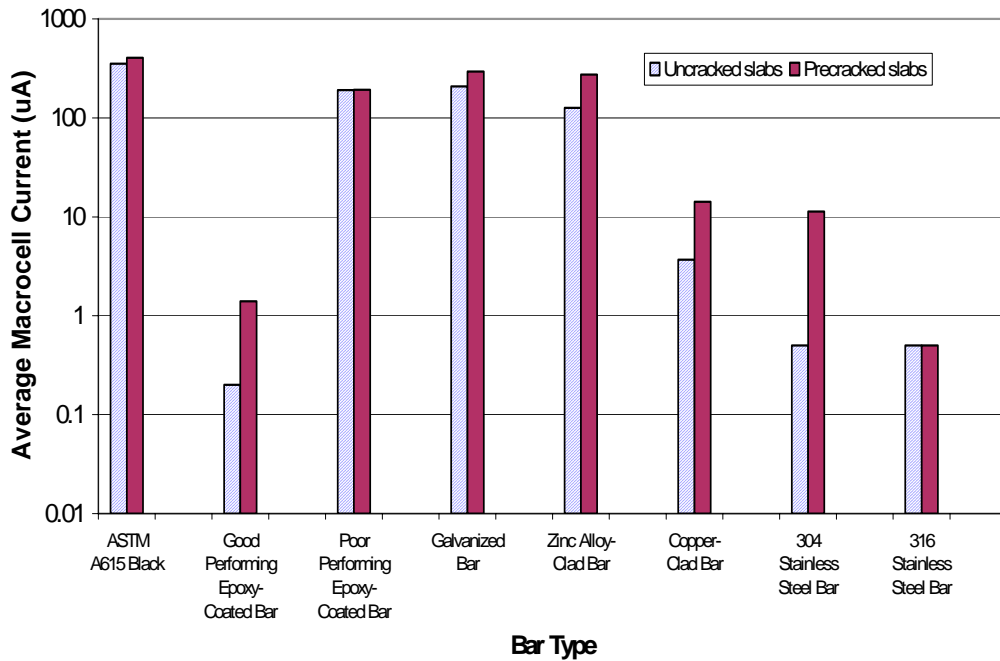
Figure 3. Average macrocell current data of eight reinforcing bar materials for 96-week SE tests
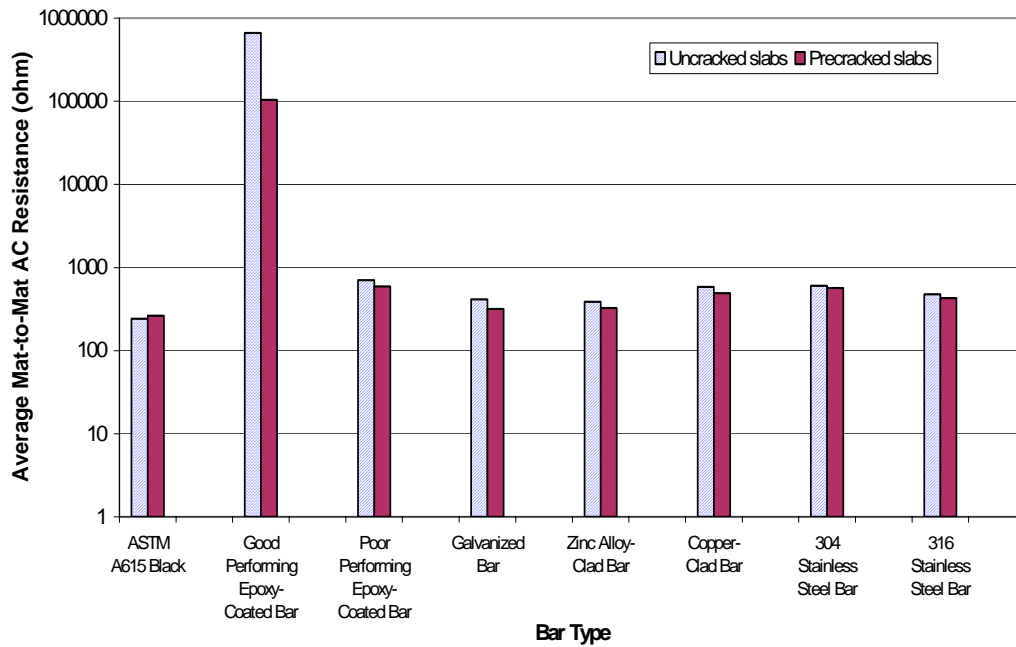
Figure 4. Average mat-to-mat AC resistance data of eight reinforcing bar materials for 96-week SE tests

Table 4. Summary of in-concrete test results per coating type[4]

Data	Slab Configuration				ECR Coating Type					
	Presence of Crack	Top Mat	Bottom Mat	Initial Defect Size (Percent)	A	B	C	D	E	F
Average Macrocell Current (uA)	Uncracked	Straight ECR	Straight black	0.5	2.5	24.6	53.8	4.8	92.5	190.7
				0.004	0.3	0.2	4.3	1.2	12.5	54.3
			Straight ECR	0.5	0.3	0.4	1.2	1.4	1.4	2.3
				0.004	0.2	0.3	0.3	1.3	0.4	5.1
		Bent ECR	Straight black	0.5	38.8	30.8	80.3	30.2	0.8	171.6
				0.004	0.5	0.4	7.9	1.9	0.4	122.0
	Precracked	Straight ECR	Straight black	0.5	59.6	65.4	103.7	11.3	151.0	191.8
				0.004	7.8	60.0	24.8	1.4	45.9	55.4
Average Mat-to-Mat Resistance (ohm)	Uncracked	Straight ECR	Straight black	0.5	3,239	3,359	1,671	3,514	1,783	787
				0.004	361,707	543,182	511,331	659,069	73,779	90,437
			Straight ECR	0.5	5,941	9,255	7,147	6,914	4,431	3,682
				0.004	488,452	561,286	528,333	941,250	259,250	479,375
		Bent ECR	Straight black	0.5	1,349	1,943	1,393	2,738	3,805	705
				0.004	13,561	97,752	171,951	68,950	167,100	57,768
	Precracked	Straight ECR	Straight black	0.5	1,281	2,918	831	1,715	822	591
				0.004	14,653	4,005	21,406	103,722	63,212	12,592

CHAPTER 2. EXPERIMENTAL METHOD

Test Specimens

Table 5 describes the test slabs employed in this study. The ECR specimens from the 96-week SE test that remained for extended outdoor exposure were coated with six different powder coating products, which were manufactured by Akzo, O'Brian, 3M, and Ajikawa (Japanese). Individual coatings were identified as Akzo-Grey™, Akzo-Green™, Akzo-Olive™, O'Brian Gold™, 3M 213, and Ajikawa.™ They are randomly designated as coatings A through F in this report. This nomenclature is identical to that in Report No. FHWA-RD-98-153.[4] As summarized in table 5, the slabs were classified into four configuration groups. These were (1) slabs containing ECR in the top mat and black bar in the bottom mat (ECR top-black bottom, 19 slabs); (2) slabs containing ECRs in both mats (ECR top-ECR bottom, 6 slabs); (3) control slabs containing black bars in both mats (black top-black bottom, 3 slabs); and (4) slabs containing straight stainless steel bars coupled with either black or stainless steel bottom bars (stainless steel, 3 slabs). Among the 19 ECR top-black bottom slabs, 6 had two 180-degree bent ECRs in the top mat, and the concrete cover of another 7 slabs was precracked over the straight bars. One specimen of each black top-black bottom and stainless top-black bottom slabs contained 180-degree bent bars in the top mat. In addition, one black and stainless slab had precracks over the top mat bars. None of the ECR top-ECR bottom slabs contained bent bars or precracks.

Every ECR bar was intentionally damaged by drilling holes through the coating to represent either 0.004 or 0.5 percent artificial coating defect using two different drill bit sizes. In every ECR top-ECR bottom slab, the two top mat ECRs contained different defect sizes, and a top mat ECR was paired with two bottom mat ECRs containing the same size of defect.

Data Collection

Corrosion progress of the top bar was monitored by both short-circuit potential (SCP) and macrocell current. SCP was measured when top and bottom bars were electrically connected. On the other hand, macrocell current was measured as the voltage drop across a 10-Ω resistor connected between the top and bottom bar mats. The current data then were converted into macrocell current density according to Ohm's law and a known surface area of 145.7 cm^2 (22.6 inch^2) for the anode (top bar). The same area was used for both coated and uncoated steel. Test data was collected periodically. During the last data measurements, additional data were collected, including the open-circuit potential (OCP) of top mat bars after the top and bottom mat bars were disconnected, the AC resistance between the top and bottom mats, and the impedance modulus ($|Z|$) at 0.1 Hertz (Hz) of top mat bars using Electrochemical Impedance Spectroscopy (EIS). Before autopsy, researchers documented the exterior condition of the test slabs using a digital camera. Photographs of the test slabs are provided in appendix A.

Table 5. Summary of test slabs exposed to outdoor weathering

Test Group	Slab ID	Bar ID	Slab Configuration		Bottom Mat	Precracked (Yes/No)
			Top Mat			
			Bar Type	Bent or Straight		
ECR Top and Black Bottom	3	3A	Coating C[1]	S	Black	N
		3B		S		N
	6	6A	Coating B[1]	S	Black	N
		6B		S		N
	15	15A	Coating D[1]	S	Black	N
		15B		S		N
	18	18A	Coating F[2]	S	Black	N
		18B		S		N
	24	24A	Coating A[1]	S	Black	N
		24B		S		N
	28	28A	Coating E[2]	S	Black	N
		28B		S		N
	7	7A	Coating A	S	Black	Y
		7B		S		Y
	13	13A	Coating C	S	Black	Y
		13B		S		Y
	14	14A	Coating E	S	Black	Y
		14B		S		Y
	19	19A	Coating F	S	Black	Y
		19B		S		Y
	21	21A	Coating D	S	Black	Y
		21B		S		Y
	25	25A	Coating B	S	Black	Y
		25B		S		Y
	30	30A	Coating C	S	Black	Y
		30B		S		Y
	1	1A	Coating D	B	Black	N
		1B		B		N
	4	4A	Coating C	B	Black	N
		4B		B		N
	8	8A	Coating F	B	Black	N
		8B		B		N
	11	11A	Coating B	B	Black	N
		11B		B		N
	22	22A	Coating A	B	Black	N
		22B		B		N
	31	31A	Coating E	B	Black	N
		31B		B		N
ECR Top and ECR Bottom	2	2A	Coating F	S	Coating F	N
		2B		S		N
	9	9A	Coating B	S	Coating B	N
		9B		S		N
	10	10A	Coating A	S	Coating A	N
		10B		S		N
	12	12A	Coating C	S	Coating C	N
		12B		S		N
	17	17A	Coating D	S	Coating D	N
		17B		S		N
	29	29A	Coating E	S	Coating E	N
		29B		S		N
Black Top and Black Bottom	5	5A	Black	S	Black	N
		5B		S		N
	23	23A	Black	B	Black	N
		23B		B		N
	20	20A	Black	S	Black	Y
		20B		S		Y
Stainless Steel	16	16A	Stainless steel	B	Black	N
		16B		B		N
	26	26A	Stainless steel	S	Black	N
		26B		S		Y
	27	27A	Stainless steel	S	Stainless steel	Y
		27B		S		N

1. Bendable coating
2. Nonbendable coating and bent bars were coated after bending

Autopsy

Autopsies were conducted in groups of four or five test slabs. A detailed autopsy of each slab was performed according to the following procedures:

Autopsy procedure for ECR

1. Rebar identification tags were attached to each test bar.
2. Digital photographs were taken to record final physical condition of the test slabs before demolition.
3. The slabs were broken open using a gas-powered saw with a diamond blade, and the bars were extracted carefully.
4. The bar surface facing the top side of the slab was marked with an arrow at one end of the bar.
5. The concrete/rebar interface was examined for corrosion products and photographed.
6. Coating defects were identified visually and with an holiday detector.
7. Using a magnifier, researchers identified coating defects, characterized these by type of defect (bare area, mashed area, crack, or holiday), and marked them with a permanent marker. Photographs were taken of both sides of each ECR to document the defects.
8. Deteriorated coating was removed with a utility knife. A knife adhesion test also was performed at six spots of undamaged coating areas to determine qualitative adhesion strength.
9. Photographs were taken of both sides of each ECR after loose (disbonded) coating was removed to document its extent of coating disbondment and assess the condition of the steel substrate beneath the removed coating.
10. The extent of removed coating was measured quantitatively.
11. Coating thickness was measured using a digital coating thickness gage.

The elapsed time between steps 6 and 11 did not exceed 1 week.

Autopsy procedure for black bars and stainless steel bars

1. Rebar identification tags were attached to each bar.
2. Photographs were taken to record final physical condition of the test slabs before demolition.
3. The slabs were broken open using a gas-powered saw with a diamond blade, and the bars were extracted carefully.
4. The bar surface facing the top of the slabs was marked with an arrow at one end of the bars.
5. The concrete/rebar interface was examined for corrosion products and photographed.
6. Photographs were taken of both sides of each bar to document the condition of the bar.
7. The bars were cleaned using chemicals and a wire brush to remove corrosion products, and corrosion damage was assessed.
8. Photographs were taken of both sides of the cleaned bars.

The elapsed time between steps 6 and 8 did not exceed 1 week.

Chloride Analysis

Concrete powder samples were taken by drilling with a 9.5-mm (3/8-inch) diameter masonry drill bit along the reinforcing steel imprints in the top mat of every slab. In addition, 14 powder samples were also collected from the selected bar imprints in the bottom mat. These powder samples were analyzed for water-soluble chloride concentration according to ASTM C1218 to determine the chloride content readily available at the bar depth. Based on the water-soluble chloride concentration analysis results, 23 samples (15 from top mat and 8 from bottom mat) were further selected and analyzed for acid-soluble chloride concentration according to ASTM C1152 to determine a relationship of water-soluble versus acid-soluble chloride concentrations.

CHAPTER 3. RESULTS AND DISCUSSION

Short-Circuit Potential and Macrocell Current Density

Tables 6 through 8 summarize the last electrochemical test data, grouped by type of test slab, that were collected in December 2002 just before the autopsy of the slabs. The data include SCP, OCP, macrocell current, AC resistance, and impedance modulus at 0.1 Hz. Figures 5 through 16 summarize the changes of mean SCP and mean macrocell current density with time for the slabs having different configurations. The elapsed time in the figures was calculated from the day when the slabs were placed in the outdoor test yard. It was noted that when test slabs had suffered from corrosion-induced physical damage, the data listed in tables 6, 7, and 8 did not represent actual condition of the reinforcing bars in those slabs.

Test slabs containing black bars in both mats

Each of the black bar test samples had cracking and delamination of the concrete cover after 96-week SE testing and before placing the slabs outdoors. Therefore, the SCP and microcell currents measured after cracking are not indicative of the true difference in performance, because the corrosion rate and potentials (SCP) drop after cracking and delamination of the concrete cover occurs. The straight, non-bent black bars had an average corrosion current density of about 2.4 μA/cm^2 (15.5 μA/inch^2) during the 96-week SE testing. Upon outdoor exposure, the black bar samples averaged somewhat less than 1.5 μA/cm^2 (9.7 μA/inch^2). This same effect may be present for some of the other poorly performing ECR samples with large damaged areas, precracks, and bending damage.

Test slabs containing ECRs in the top mat and black bars in the bottom mat

Test slabs containing ECRs performed better, especially the ones with smaller initial defect size (0.004 percent), than the black bar control slabs because ECRs exhibited lower macrocell current and more positive SCP over the test period than those of the black bar counterparts. Macrocell current density of the black bars became negative in every category after 1,600 days (see figures 6, 8, and 10). Negative current readings indicated reversal of macrocell current between original anode (top mat) and original cathode (bottom mat) at the time of measurement. Such current reversal was caused by corroding bottom mat cathode steel first instead of usual corrosion initiation at the top mat bars. This situation was possible when chloride reached the black bars in the bottom mat and subsequently initiated the active corrosion there, while top mat ECRs were able to suppress corrosion. As discussed later, chloride concentration at some bottom bar depths was found to far exceed the chloride threshold for corrosion initiation of black bars (250 to 300 ppm).

Test slabs containing ECRs in both mats and stainless steel

Figures 11 and 12 show variations of mean SCP and macrocell current density with time for the slabs containing either ECRs in both mats or stainless steel. There were three test slabs containing stainless steel bars in the top mat or in both mats, and two of them were precracked.

Because of the small number of slabs, the stainless steel slabs were treated as one variable, even though some contained cracks and/or black bottom bars. Each pair of ECRs in the top and bottom mats contained the same coating damage (0.004 or 0.5 percent), and every slab contained two pairs of ECRs with each of the two coating defect areas. While the 0.5 percent damaged ECRs exhibited more negative potentials compared to the others (ECRs with 0.004 percent coating defect and stainless steel) during most of the exposure time, all of the mean macrocell current density data remained very small throughout the test period. Mean macrocell current density of stainless steel bars with black bottom steel became negative at around 1,600 days due to active corrosion in the bottom black mat. Furthermore, when ECR was used in both mats, the coating defect size did not make a noticeable difference in macrocell current density output, which approached that of stainless steel bars. This observation suggests that using ECRs in both mats in northern bridge decks is likely to give very high corrosion resistance in corrosive environments under deicing salt applications, and may approach an equivalent corrosion resistance to that offered by stainless steel bars.

Effect of precrack

The effect of having precracks on SCP and macrocell current density can be seen in figures 13 and 14, which show the change of mean SCP and mean macrocell current density with time for the slabs containing straight black bars and straight ECRs, respectively. All the top bars were connected to black bottom bars. In general, mean SCP and macrocell current density data for black bars and top mat ECRs behaved similarly in precracked and uncracked concrete during the outdoor weathering test period. The presence of the precrack influenced the time-to-corrosion initiation during the initial 96 weeks of SE testing more than after long-term outdoor exposure.

Effect of bent ECR

Figures 15 and 16 show the change of mean SCP and mean macrocell current density with time for straight and bent ECRs in uncracked concrete, respectively. Test slabs containing ECRs in both mats exhibited the most negative mean SCP among three groups, however, the performance between the groups was not largely different. When bent ECRs were connected to the black bottom bars, they produced the highest mean macrocell current density and were followed closely by the straight ECRs coupled with black bottom bars. In contrast, test slabs containing straight ECRs in both mats exhibited insignificant mean macrocell current density throughout the entire exposure period.

Further data analysis related to slab configuration and bar type

Table 9 summarizes the mean values of the test data presented in figures 5 through 12 according to four bar types (black, stainless steel, ECR with 0.5 percent initial coating damage, and ECR with 0.004 percent initial coating damage) and five slab configurations (straight top-black bottom-uncracked, straight top-ECR bottom-uncracked, straight top-black bottom-precracked, bent top-black bottom-uncracked, and stainless steel bars in uncracked).

The SCP and macrocell current density data listed in table 9 also are presented in figures 17 and 18, respectively. As shown in figure 17, black and stainless steel bars exhibited the most

negative and positive mean SCP, respectively. Mean SCP of the black bars moved in the negative direction when slabs contained precracks and bent bars. When coating defect size decreased from 0.5 to 0.004 percent, the mean SCP became more positive (lower corrosion tendency). As observed in figures 5 through 16, mean macrocell current density varied significantly depending on slab configuration and bar type. This trend is summarized in figure 18. The black bars produced the highest mean macrocell current density among various combinations of test variables regardless of slab configuration, i.e., presence of crack and bar shape (bent vs. straight).

To illustrate relative significance of slab configuration and bar type on the mean macrocell current density, figure 19 presents the ratios of macrocell current density data shown in table 9 and figure 18 by dividing them by the highest average value (1.3 µA/cm^2 (8.4 µA/inch^2)) of the black bent bar-black bottom-uncracked concrete slabs. The stainless steel bars exhibited negligible mean macrocell current density which was only 1 percent of the highest black bar case. For straight ECRs, the mean macrocell current density was influenced by the size of the initial coating damage and whether the bottom mat bar was coated or uncoated. When straight ECRs in the top mat were coupled with black bars in the bottom mat, the size of coating defect became a factor for controlling macrocell current density. In the case of straight top ECRs containing 0.004 percent of initial coating defect coupled with black bottom bars, mean macrocell current density was 7 to 21 percent of the highest black bar case, depending on the presence of precracks. If straight top ECRs contained 0.5 percent initial coating defect, the current values increased to more than 40 percent of the highest black bar case, regardless of whether the slab had a precrack. For bent ECRs, even ones containing 0.004 percent coating damage produced noticeable macrocell current density when they were connected to black bottom bars, such that mean macrocell current density increased to 38 and 49 percent of the highest black bar case, regardless of initial coating defect size. If top mat ECRs were connected to ECRs in the bottom mats in uncracked concrete, the effect of coating damage on macrocell current density was minor, and the ratio decreased to no greater than 2 percent of the highest black bar data. They behaved similarly to stainless steel bars.

Figure 20 shows the effect of coating defect size on macrocell current density for ECRs in top mat only and ECRs in both mats cases. A regression analysis shows a well-defined relationship, indicating that defect size makes a significant influence on the ECRs coupled with black bottom bars, but the coating size effect is diminished when ECRs are used in both mats.

Effect of coating type

Table 10 lists mean SCP and mean macrocell current density data per coating type. The same data are presented in figures 21 and 22. Because of a large variation among different coating types, mean macrocell current density is presented in two scales: a linear scale in figure 22(a) and a logarithmic scale in figure 22(b). Performance differences are difficult to interpret from the SCP data in figure 21. Generally, coatings C and F had the worst SCP data, while coatings A, D, and E had the best SCP data. It can be seen in figure 22 that mean macrocell current density varied significantly by coating type, which could be related to coating quality, but such variation disappeared when ECRs were used in both mats. Coatings A and D performed well in

all configurations, while coatings C and F had generally poor performance (except for the case of ECRs in both mats).

Statistical Analysis of Test Data

A statistical analysis was conducted to calculate sample mean ($\bar{x}$) and sample standard deviation (*s*) for SCP, macrocell current density, AC resistance, and impedance modulus at 0.1 Hz data. Then, the results were used to determine the 95 percent confidence interval for the unknown population mean (μ). The 95 percent confidence interval for μ means that researchers are 95 percent confident that the unknown μ is within this interval for a variable. Statistical analysis was performed for the variables classified by combinations of slab configuration and bar type, and the final results are provided in figures 23 through 26.

Figure 23 shows the distribution of μ for the SCP data categorized by 12 combinations of test variables. The μ's are evenly distributed among different variables. The stainless steel bars and bent black bars exhibited the most positive and most negative SCP mean values, respectively.

Figure 24 shows distribution of μ's for the macrocell current density data categorized by 12 combinations of test variables. As noted in earlier sections, use of stainless steel bars and ECRs containing 0.004 percent initial coating damage produced the least current density. When ECRs having 0.5 percent initial coating defect are used in both mats, the macrocell current density slightly increased from zero. These are followed by straight ECRs containing 0.004 percent coating defects in the top mat only and other top mat only ECR cases. The black bar cases yielded the highest mean values.

High coating resistance and impedance is characteristic of a quality, corrosion-resistant coating. Figures 25 and 26 show distribution of μ's for AC resistance measured between the two mats and impedance modulus at 0.1 Hz of top mat bar, respectively. Impedance modulus data exhibited larger variations and higher absolute values than did the AC resistance test data. The four highest upper limits of μ's were achieved by ECRs containing 0.004 percent coating defect. However, the lowest limit of μ's was near zero resistance for most combinations of test variables.

Autopsy Results

Researchers began test slab autopsies by making a 1.3-cm (0.5-inch) deep groove along the bottom side of the slabs at two locations (figure 27) using a gas-powered saw. A test slab was split into several fragments by using a chisel and hammer. Embedded bars were then carefully extracted using a small chisel and hammer (figure 28). Researchers exercised caution when removing ECRs to avoid coating damage.

Figure 29 shows a photograph of a top mat straight ECR that performed well throughout the severe testing regime. The ECR and concrete/bar interface appearance was excellent, with no sign of corrosion. Figure 30 shows a severely corroded, straight, top mat ECR. Figures 31 and 32 show photographs of well and poorly performing bent ECRs, respectively, both from the top mat.

Closeup examination of the extracted ECRs revealed four different coating conditions, which are shown in figure 33. When the ECR performed well, the exposed coating looked new with a glossy texture (figure 33(a)). It was observed that when the epoxy coating reaches the advanced stage of deterioration due to corrosion, the coating exhibits numerous hairline cracks (figure 33(b)) and then blisters (figure 33(c)). Accumulation of multiple rust layers beneath disbonded coating was also a common corrosion morphology observed on severely corroded ECRs (figure 33(d)). The disbonded coating mentioned above was defined as a permanently separated coating from substrate upon knife adhesion test performed several days after the ECRs were excavated. Therefore, it was different from temporary adhesion loss, which can recover fully or partially with time.

Figures 34 and 35 show photographs of a severely corroded straight black bar and a poorly performed bent black, respectively. Figure 36 shows a photograph of a broken test slab fragment, which exhibited active corrosion in the bottom black bar mat.

All of the extracted bars, including those in the bottom mat, were carefully documented, cleaned, and examined according to the autopsy procedure described. Figures 37 and 38 show photographs of autopsied bars taken after they were cleaned. The bars shown in figure 37 were removed from slab #18, which contained ECRs in the top mat only. While one top ECR (the second bar from the top in the photograph) exhibited localized coating disbondment originated from corrosion at the smaller artificial coating defects (0.004 percent), the other top ECR (the first bar from the top in the photograph) experienced severe corrosion, again initiated at the larger artificial coating defects (0.5 percent), such that the epoxy coating could be peeled off completely.

The bars shown in figure 38 were removed from slab #10, which contained ECRs in both mats. While one top ECR (the second bar from top in the photograph) exhibited virtually no reduction in adhesion even at the smaller artificial coating defects (0.004 percent), the other top mat ECR (the first bar from top in the photograph) experienced moderate corrosion that initiated at the larger artificial coating defects (0.5 percent), such that epoxy coating could be peeled off locally around the initial defects. The ECRs extracted from the bottom mat were corrosion-free and had minimal adhesion loss. The photographs of individual autopsied bars are included in appendix A.

Tables 11 and 12 summarize the findings of the autopsied ECRs in terms of the number of final defects, coating thickness, exterior physical appearance, knife adhesion, and degree of adhesion loss. Final defects were classified as bare area, mashed area (mechanical damage), coating crack, and holiday. The number of final coating defects on the autopsied ECRs was very large on some poorly performing bars, while others maintained good coating continuity. The coating cracks as shown in figure 33 were the most frequent form of coating deterioration. When the coating defects were too excessive to count individual defects, an arbitrary number of 100 was assigned to quantify the worst condition in the subsequent data analysis.

Figures 39 through 42 present the 95 percent confidence intervals for µ of the data provided in tables 11 and 12. Each plot was constructed for 10 combinations of test variables. It is

statistically significant that the ECRs removed from the bottom mat of the ECR top-ECR bottom slabs exhibited the least number of final defects (figure 39) and the best appearance (figure 40). The bottom mat ECRs extracted from these slabs also exhibited the strongest knife adhesion (figure 41) and the least amount of coating disbondment (figure 42). Their performance was followed by the top mat straight ECRs containing 0.004 and 0.5 percent coating defects, respectively. Conditions of top mat ECRs that were removed from the ECR top-ECR bottom slabs were not particularly different from those of the top mat only cases. Based on macrocell current density data and autopsy results, the excellent performance of test slabs containing ECRs in both mats should be attributed to the fact that the presence of ECR in the bottom mat suppresses the corrosion activity by minimizing the cathodic reaction (oxygen reduction through consuming electrons). In general, bent ECRs, when coupled with black bottom bars, performed the worst of all materials tested.

Chloride Analysis

Tables 6 through 8 list the water-soluble chloride data for every bar in the top mat. Based on the reversal of macrocell current and the high level of chloride in the top mat, some slabs were selected for additional chloride analysis at the bottom mat. To estimate the total chloride, limited acid-soluble chloride analysis also was conducted, with the selected powder samples representing various concentrations of water-soluble chloride. Figure 43 shows a result of the regression analysis demonstrating a relationship between water-soluble vs. acid-soluble chloride concentration. Regression analysis of the experimental chloride data indicates that the water-soluble chloride concentration of the concrete is approximately 89 percent of the total (acid-soluble) chloride concentration. Coarse aggregates used in this project came from Eau Claire, WI. Because these aggregates did not contain chlorides, the acid-soluble (total chlorides) and water-soluble (free chlorides) test results were similar.

Figure 44 shows the 95 percent confidence intervals for μ for 10 combinations of test variables. It is interesting to note that water-soluble chloride concentration in the top mat containing black bars was far lower than the rest. This is likely due to the fact that the slabs containing black bars were cracked and delaminated after the 96-week SE testing and before being placed outdoors. Rainwater passing through the cracks and delaminations likely dissolved some of the free chloride ions in the concrete near the top mat of steel. Compounding of the free chloride in the black bar rust products also may have occurred.
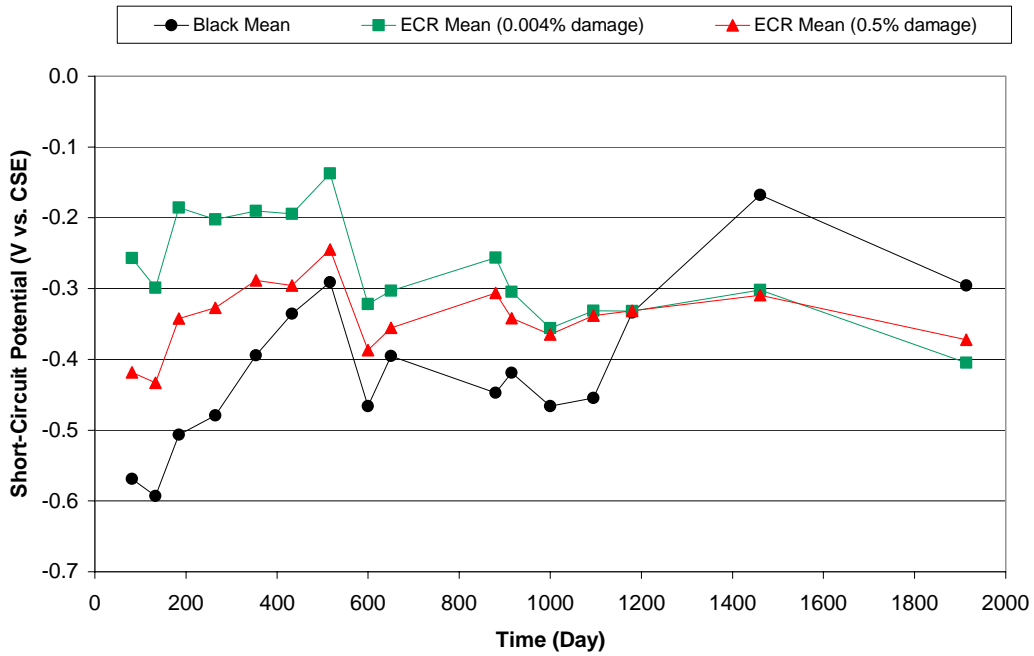
Figure 5. Short-circuit potential change with time (straight top (black and ECR)-black bottom-uncracked concrete) during outdoor exposure
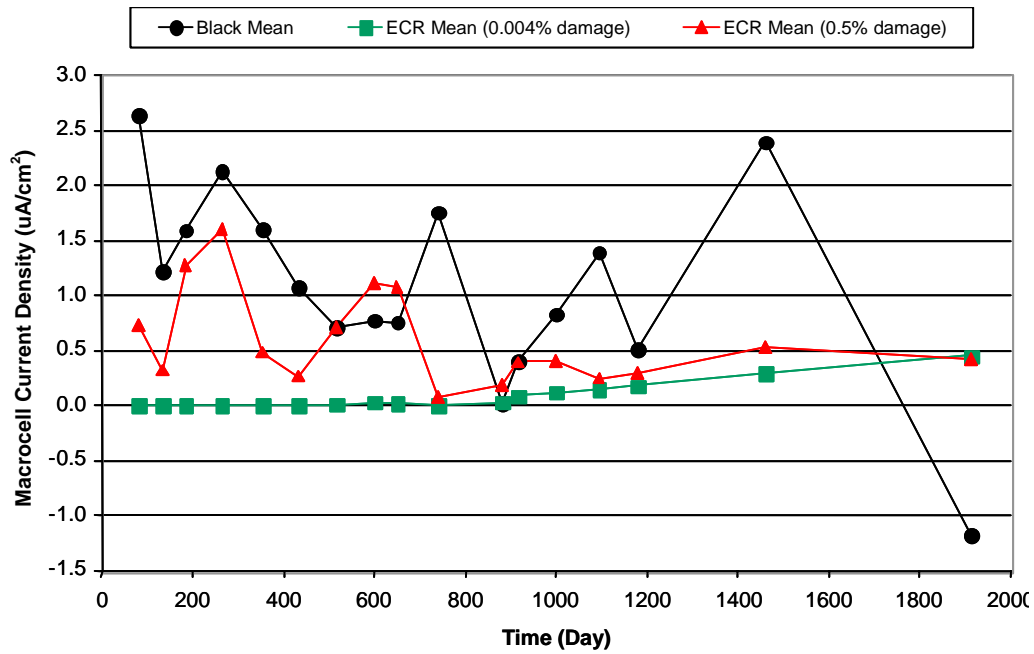
Figure 6. Macrocell current density change with time (straight top (black and ECR)-black bottom-uncracked concrete) during outdoor exposure

21
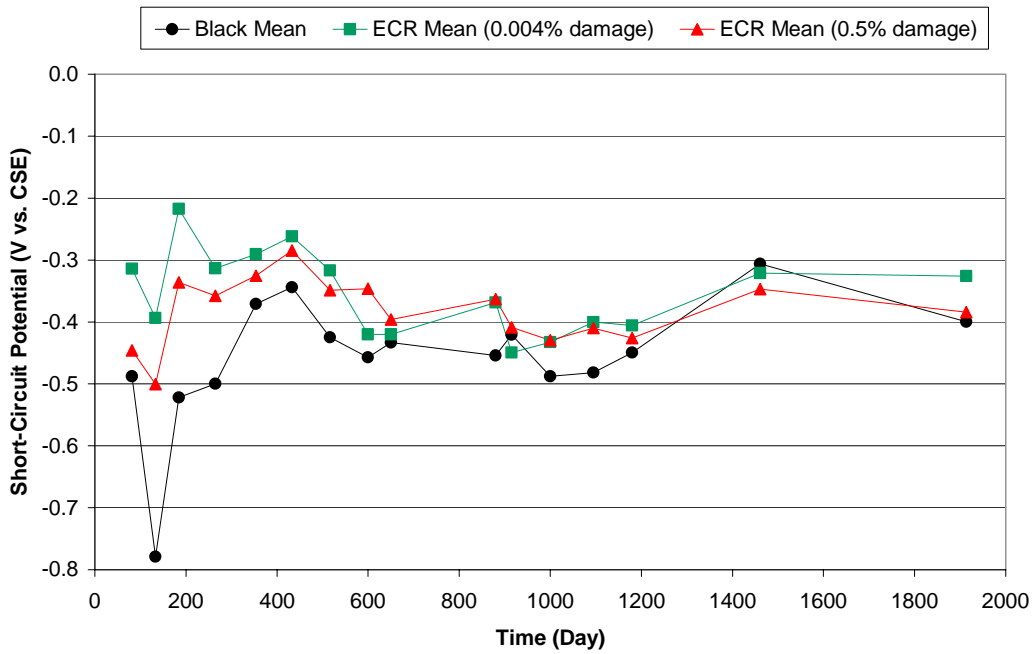
Figure 7. Short-circuit potential change with time (straight top (black and ECR)-black bottom-cracked concrete) during outdoor exposure
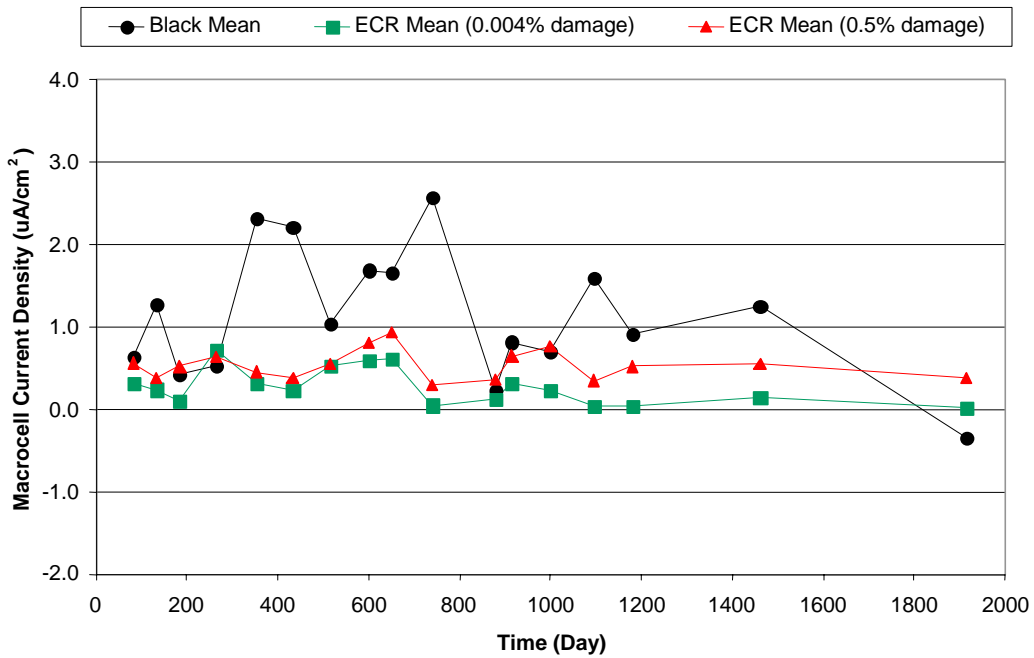
Figure 8. Macrocell current density change with time (straight top (black and ECR)-black bottom-cracked concrete) during outdoor exposure
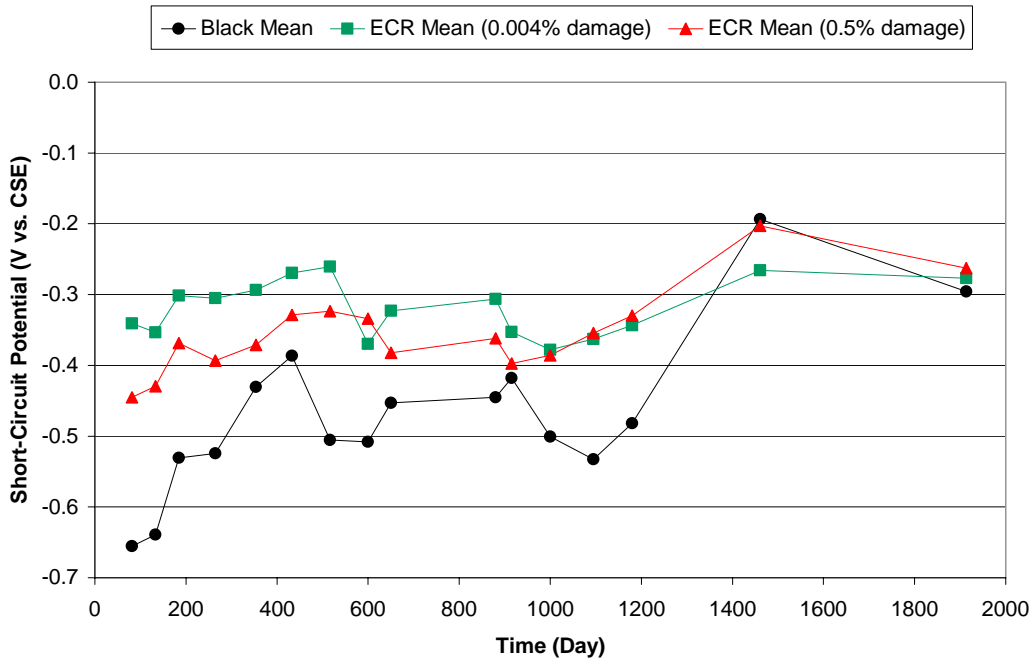
Figure 9. Short-circuit potential change with time (bent top (black and ECR)-black bottom-uncracked concrete) during outdoor exposure
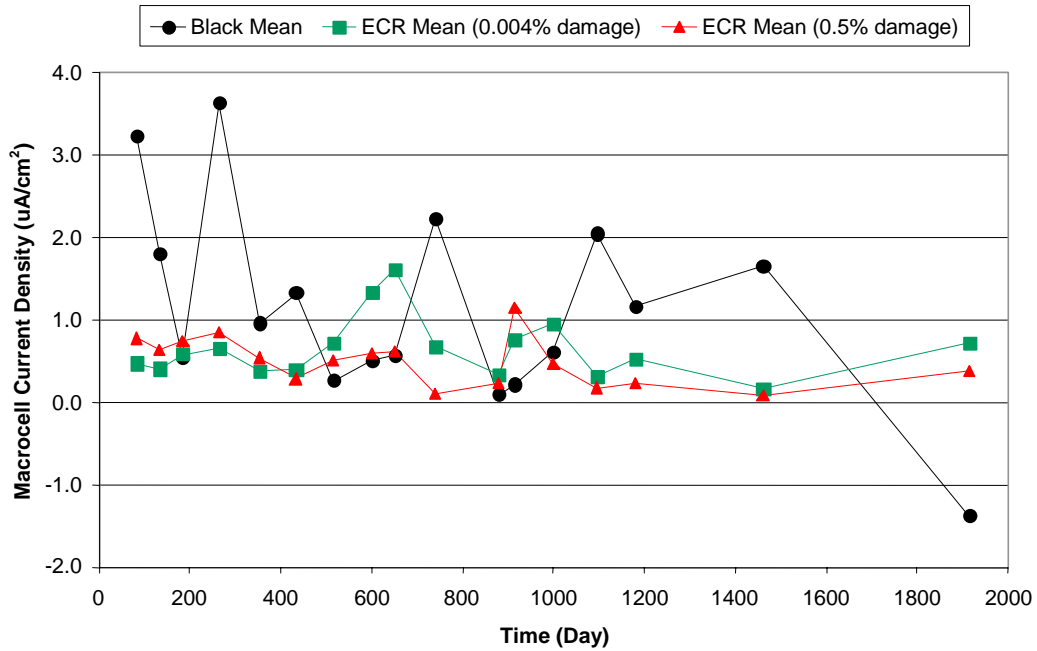
Figure 10. Macrocell current density change with time (bent top (black and ECR)-black bottom-uncracked concrete) during outdoor exposure
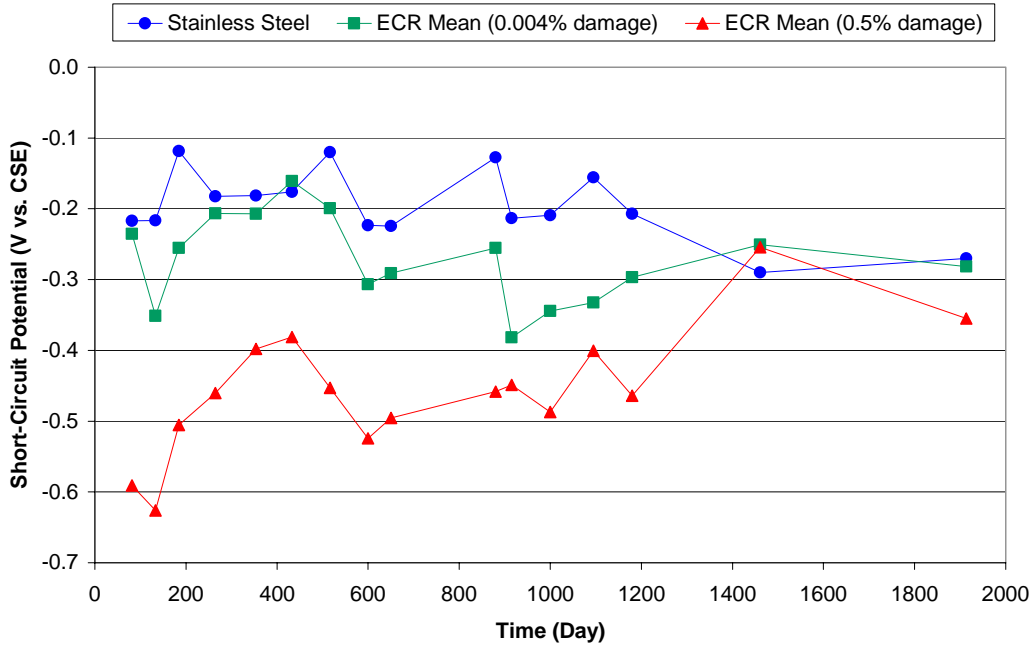
Figure 11. Short-circuit potential change with time (stainless steel and ECR in both mats-uncracked concrete)
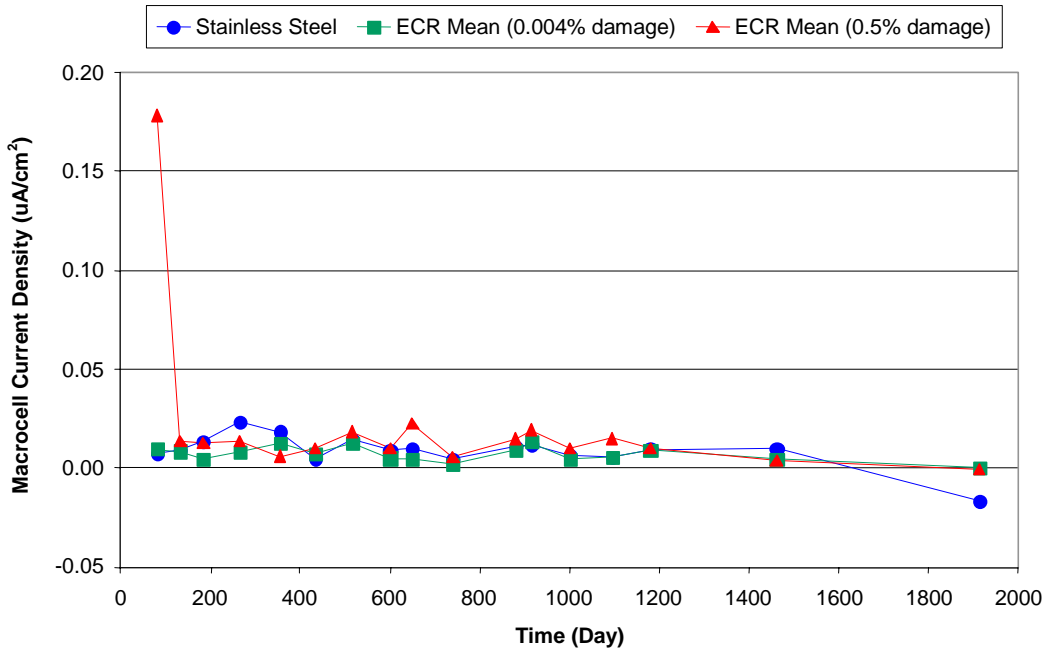
Figure 12. Macrocell current density change with time (stainless steel and ECR in both mats-uncracked concrete)

24
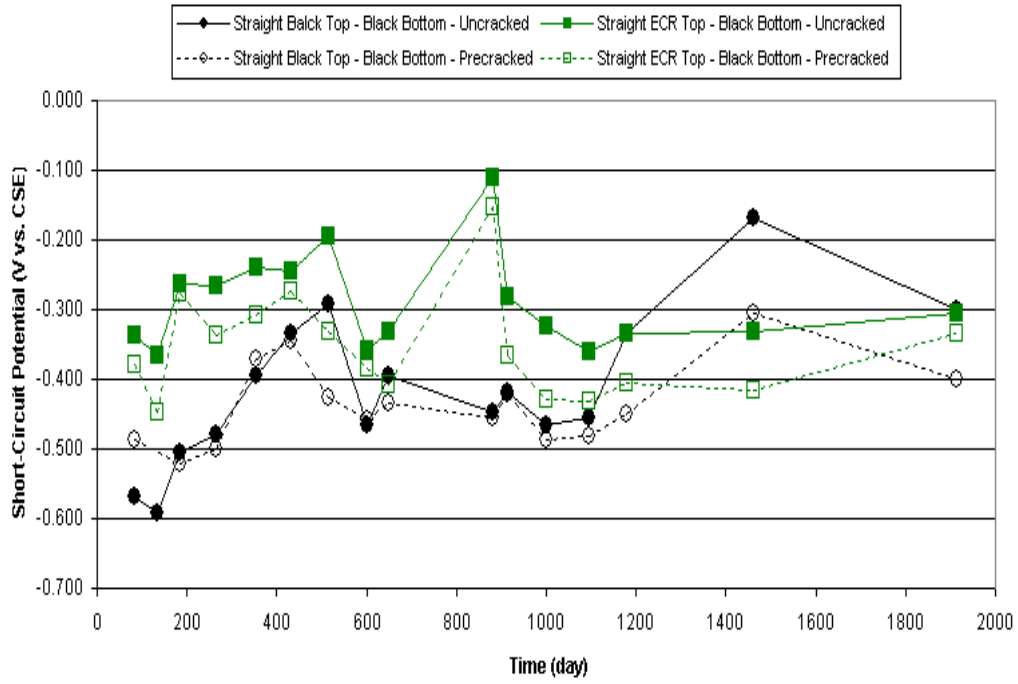
Figure 13. Mean short-circuit potential change with time (uncracked vs. precracked concrete)
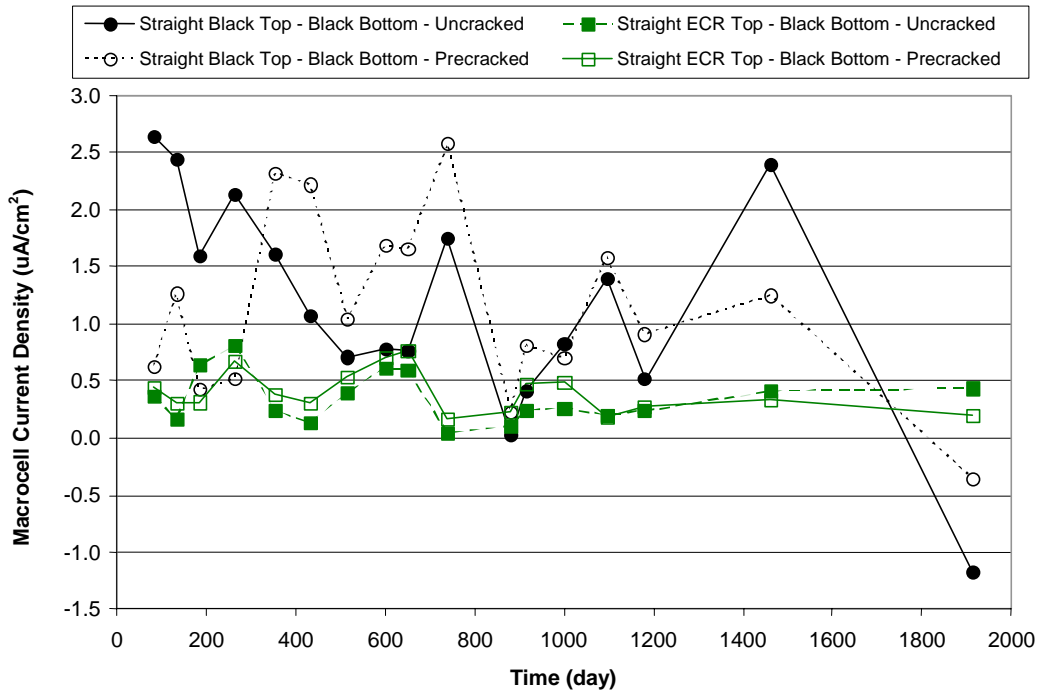
Figure 14. Mean macrocell current density change with time (uncracked vs. precracked concrete)

25
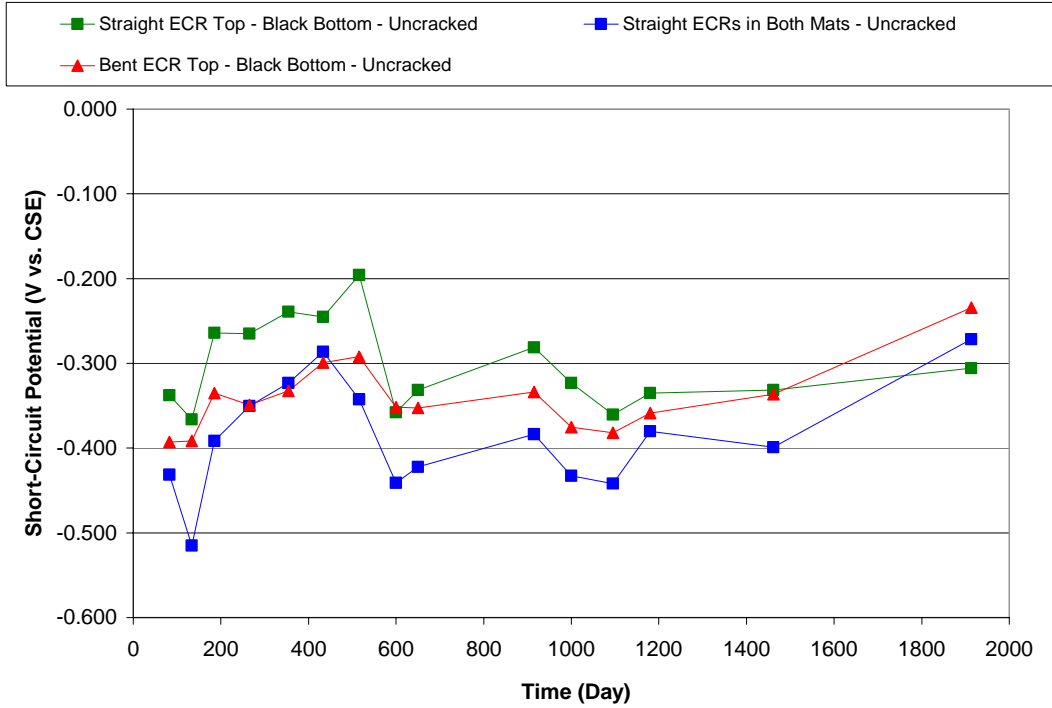
Figure 15. Mean short-circuit potential change with time (straight vs. bent ECRs in uncracked concrete)
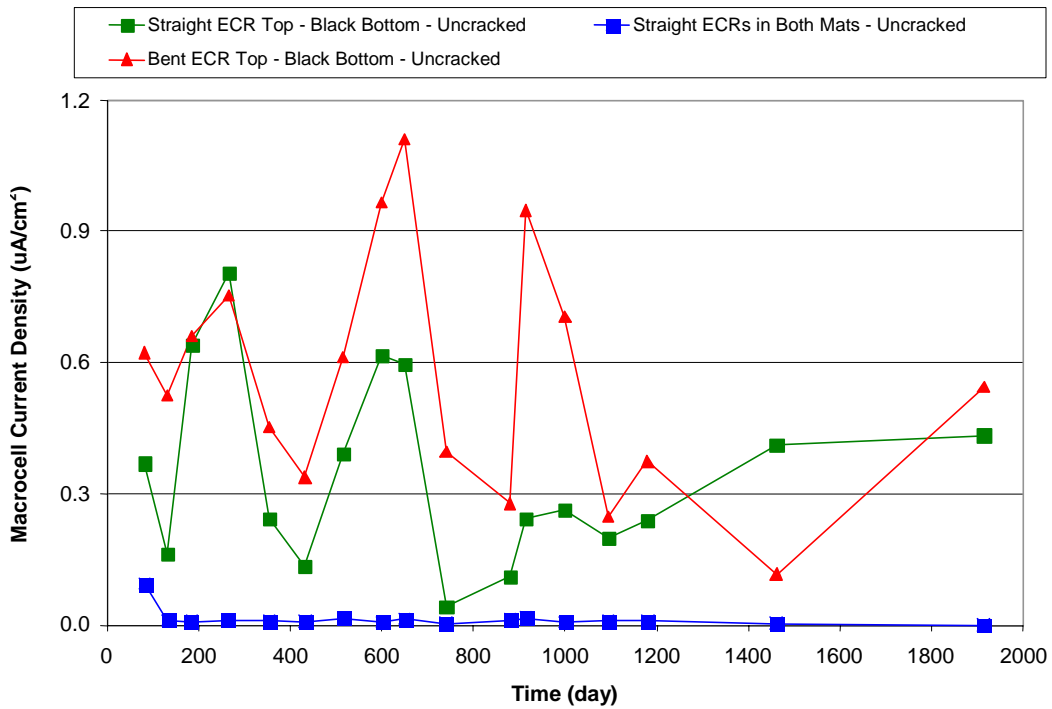
Figure 16. Mean macrocell current density change with time (straight vs. bent ECRs in uncracked concrete)
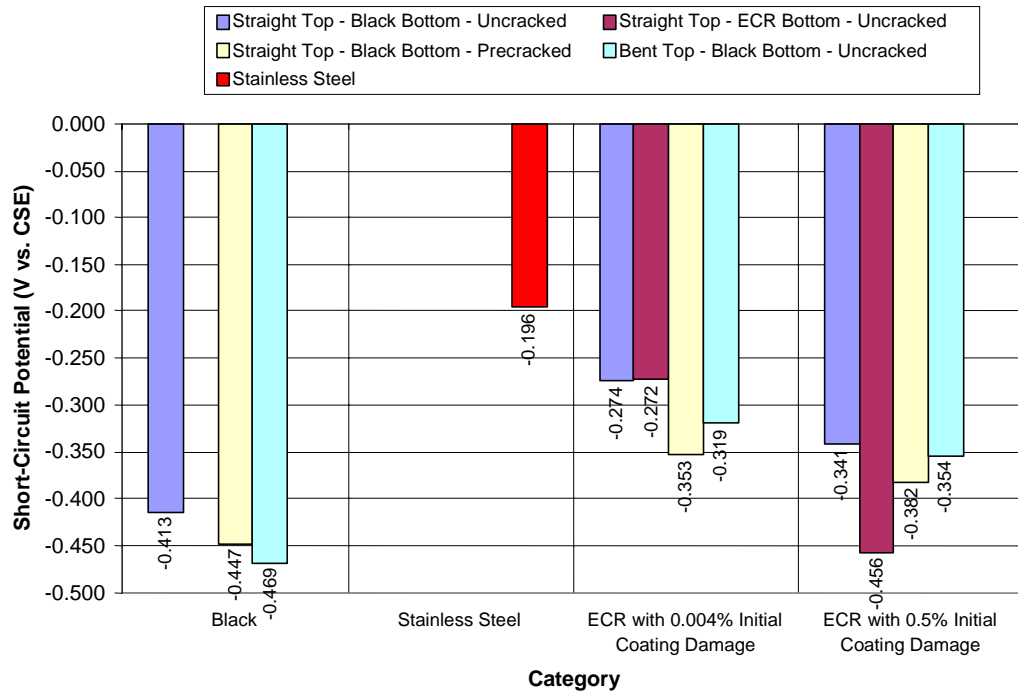
Figure 17. Mean short-circuit potential data classified by bar type (from table 9)
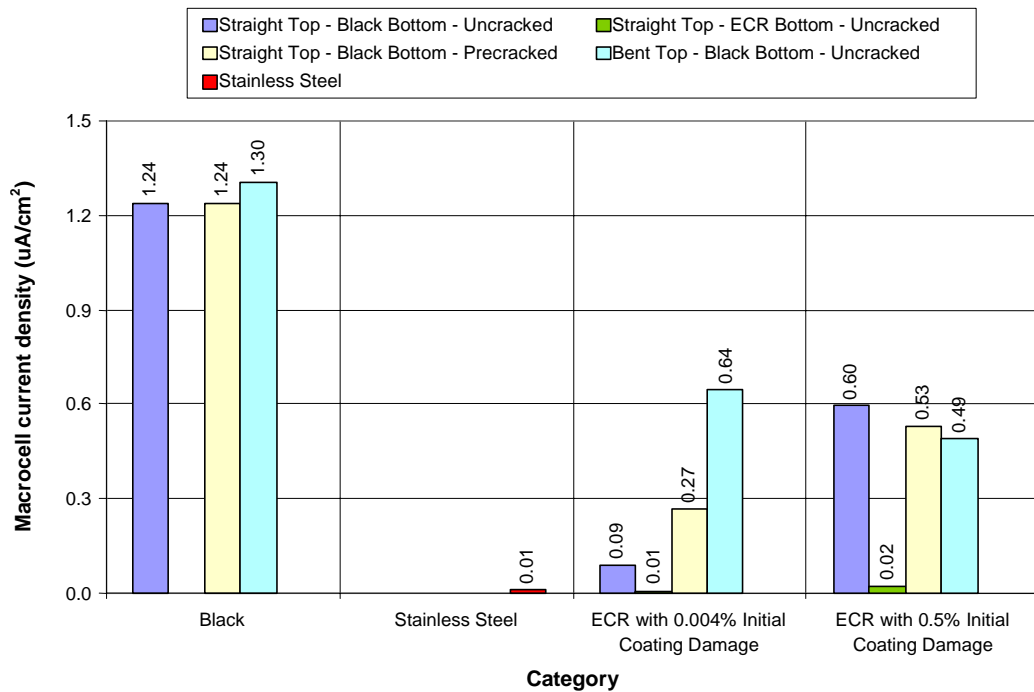
Figure 18. Mean macrocell current density data classified by bar type (from table 9)
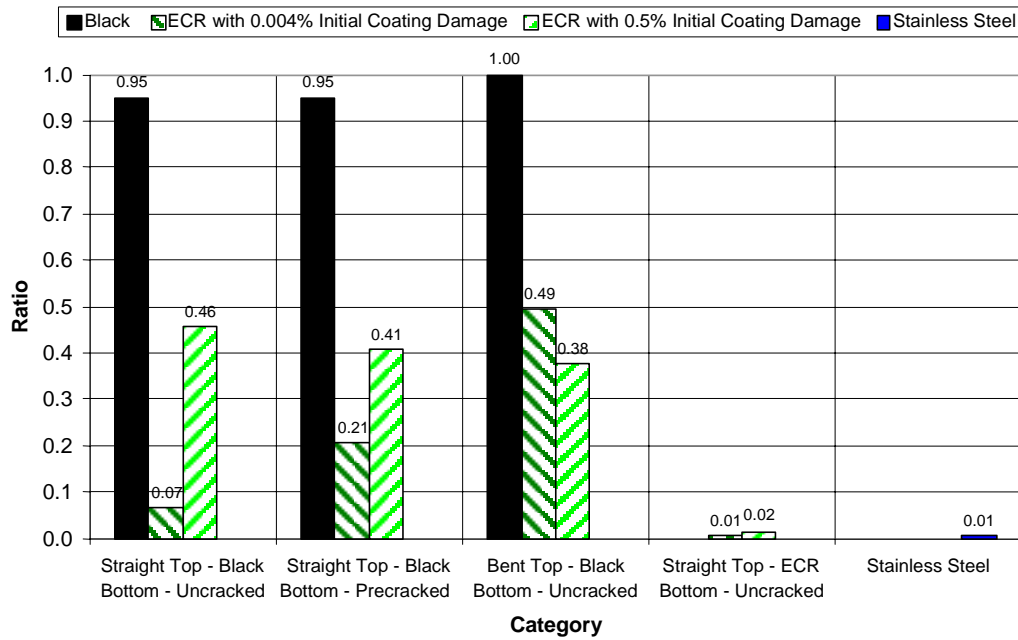
Figure 19. Relative ratio of macrocell current density per slab configuration
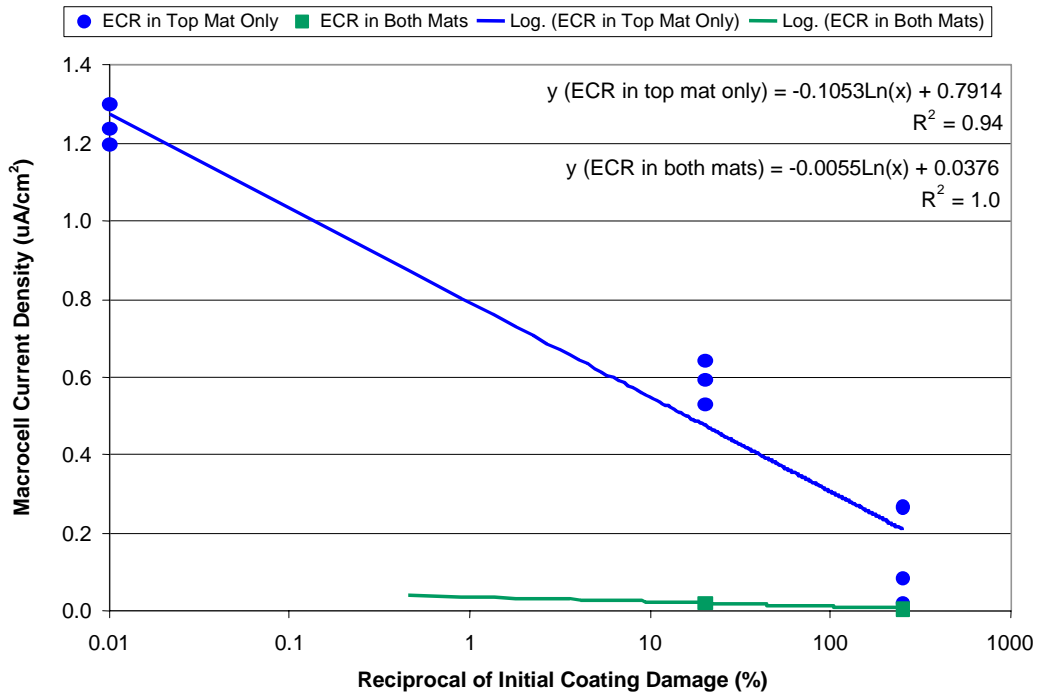
Figure 20. Relationship between macrocell current density versus initial artificial coating defects

28
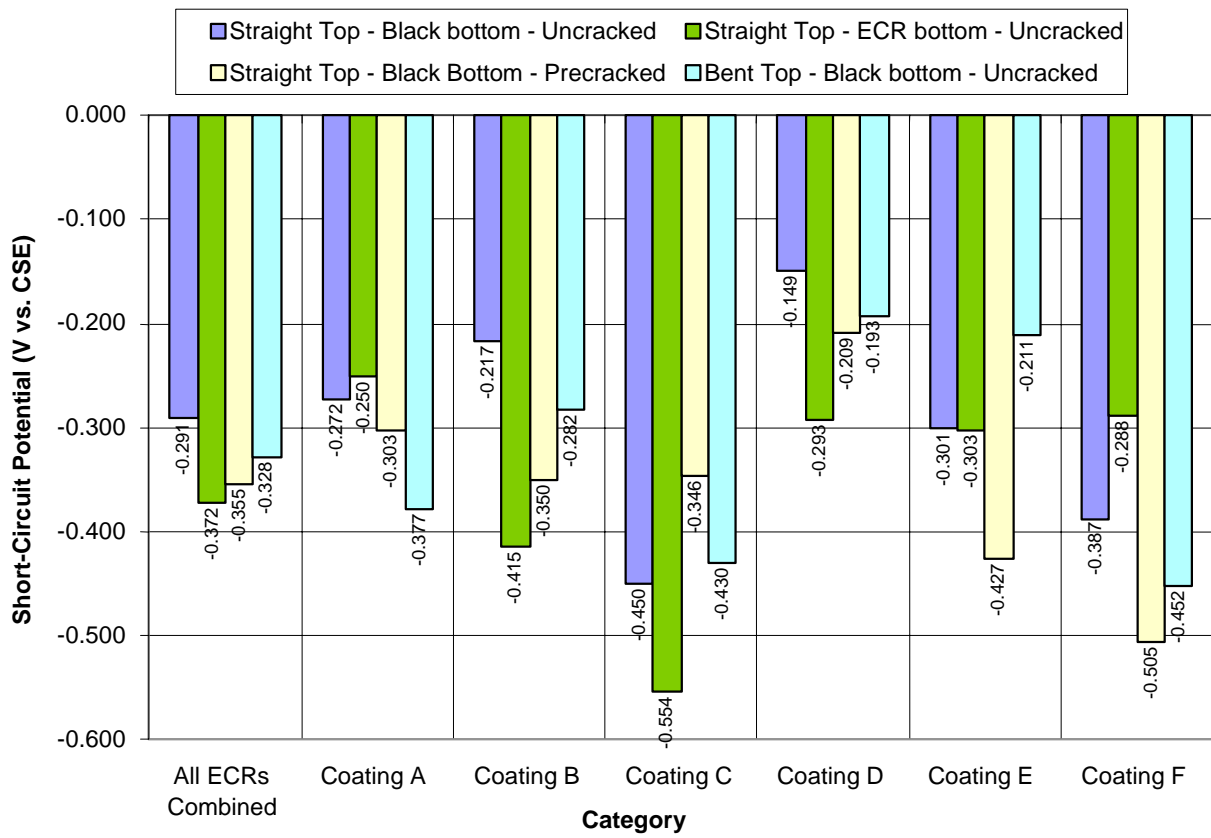
Figure 21. Short-circuit potential data classified by coating type
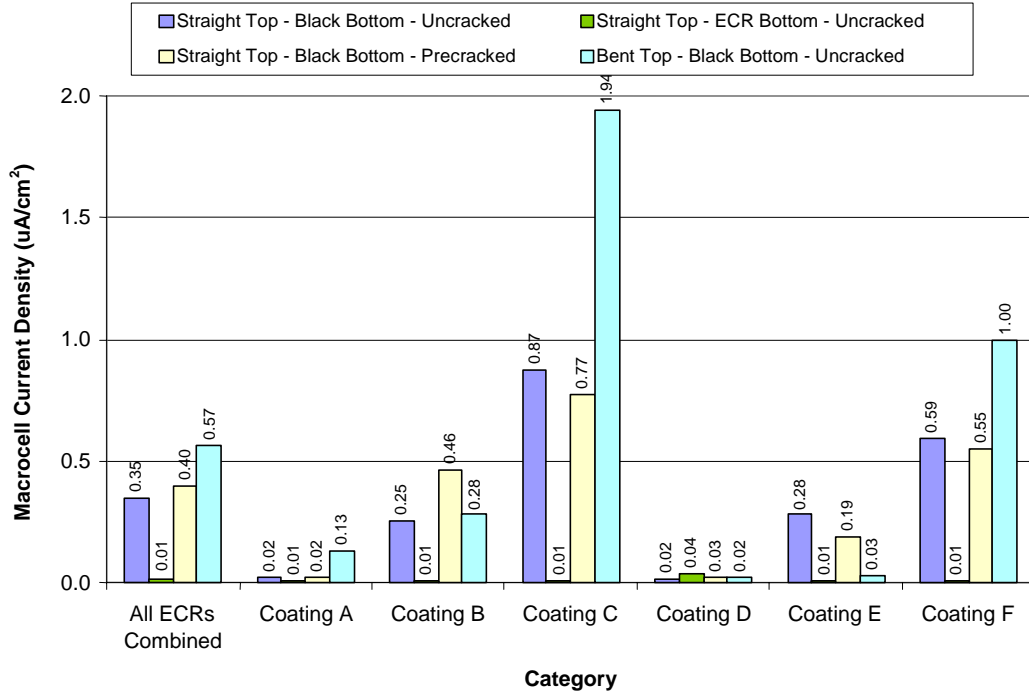
Figure 22(a). Macrocell current density data classified by coating type (linear scale)
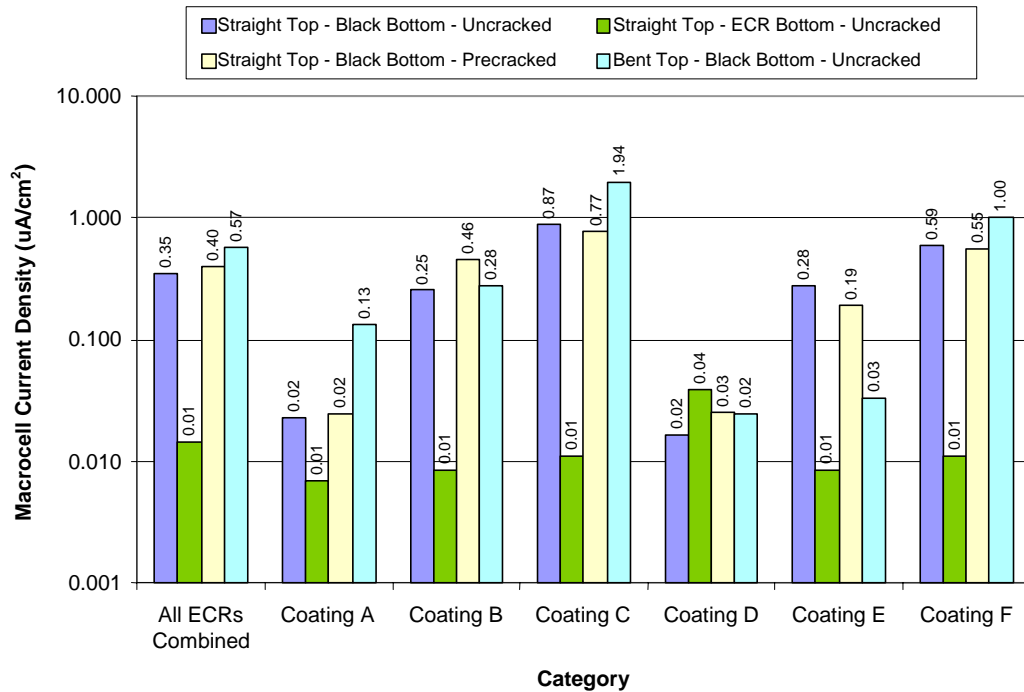
Figure 22(b). Macrocell current density data classified by coating type (logarithmic scale)
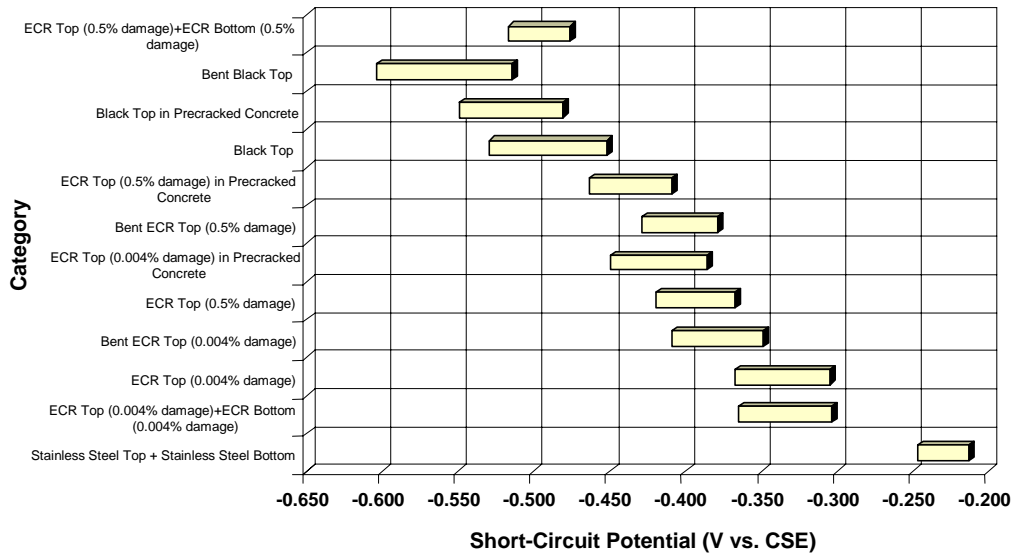
Figure 23. Ninety-five percent confidence intervals for short-circuit potential data
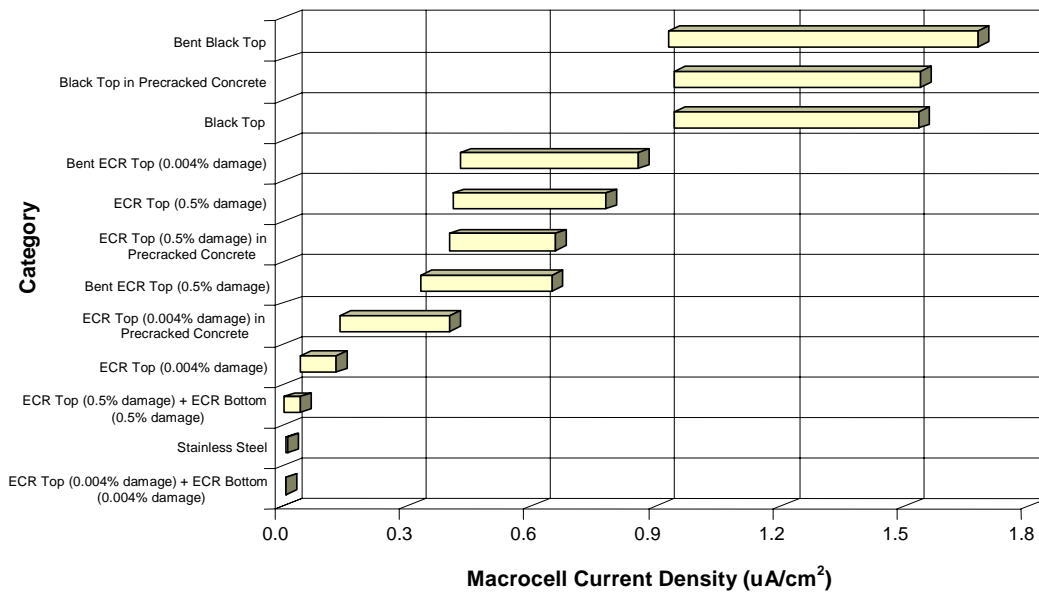
Figure 24. Ninety-five percent confidence intervals for macrocell current density data
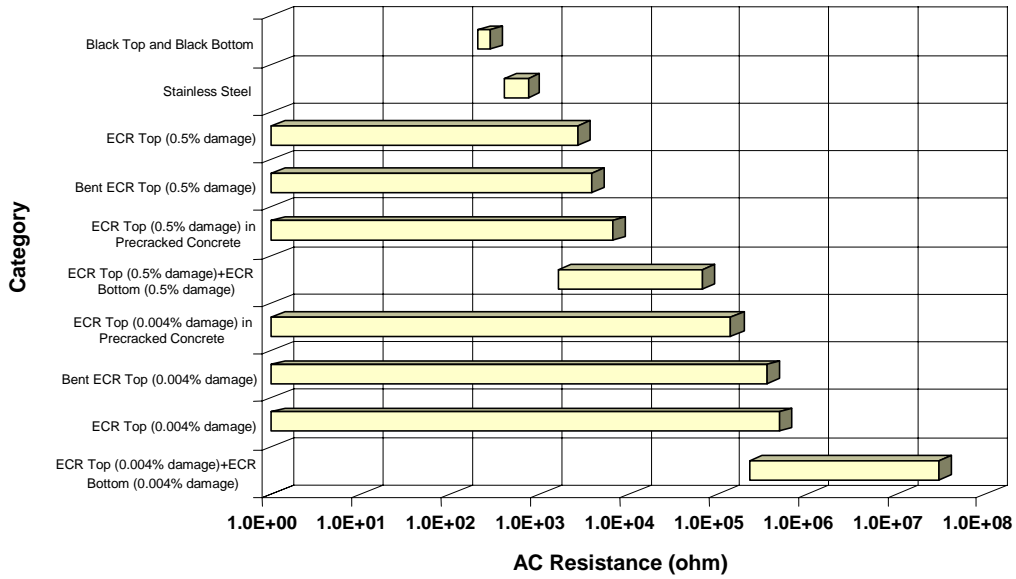
Figure 25. Ninety-five percent confidence intervals for AC resistance data
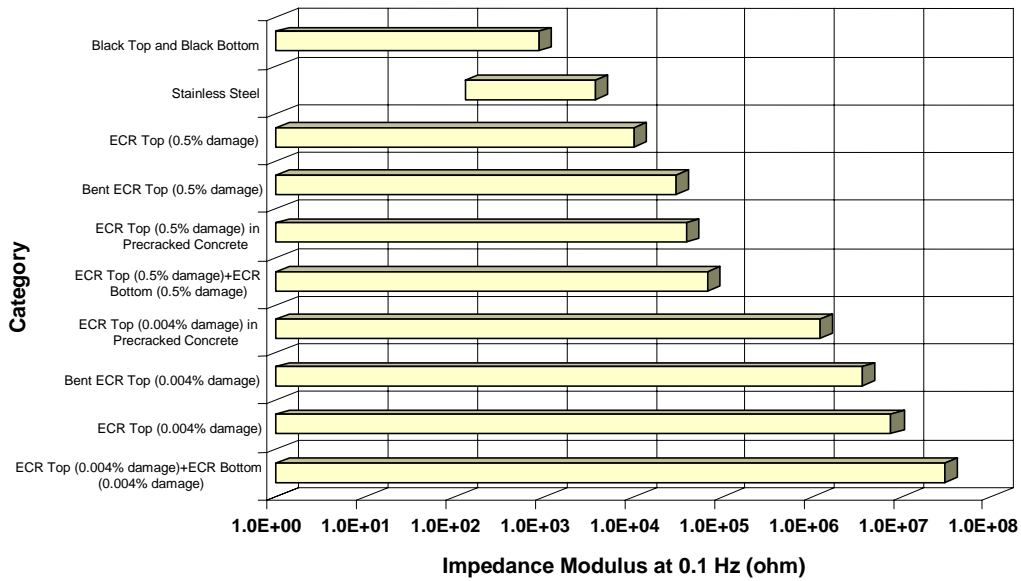
Figure 26. Ninety-five percent confidence intervals for impedance modulus data

Figure 27. Cutting a test slab with a gas-powered saw

Figure 28. Extraction of embedded reinforcing bars

Rebar imprint

7B-T

Figure 29. Typical condition of ECR with good corrosion resistance (slab #7—top right bar)

30B-T

Rebar imprint

Figure 30. Typical condition of ECR with poor performance (slab #30—top right bar)

Figure 31. Typical condition of a bent ECR with good performance (slab #1—top left bar)

Figure 32. Typical condition of a bent ECR with poor performance
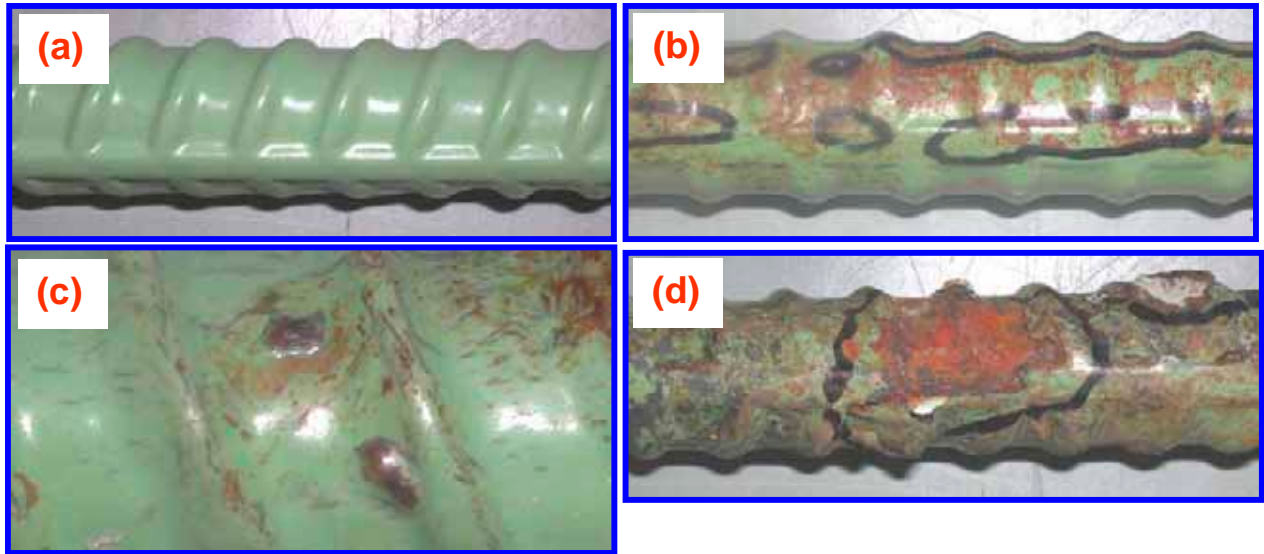
Figure 33. Closeup views of ECRs exhibiting various conditions: (a) an intact ECR; (b) an ECR containing hairline coating cracks; (c) an ECR containing coating blisters and hairline coating cracks; and (d) a delaminated ECR revealing severely corroded substrate

Figure 34. Typical condition of black bars in the top mat

Figure 35. Typical condition of black bent bars in the top mat (slab #23—top right bar)

Figure 36. Corroded bottom mat (slab #19)

Figure 37. Photograph of autopsied bars extracted from slab #18 (ECR top-black bar bottom)

Figure 38. Photograph of autopsied bars extracted from slab #10 (ECRs in both mats)
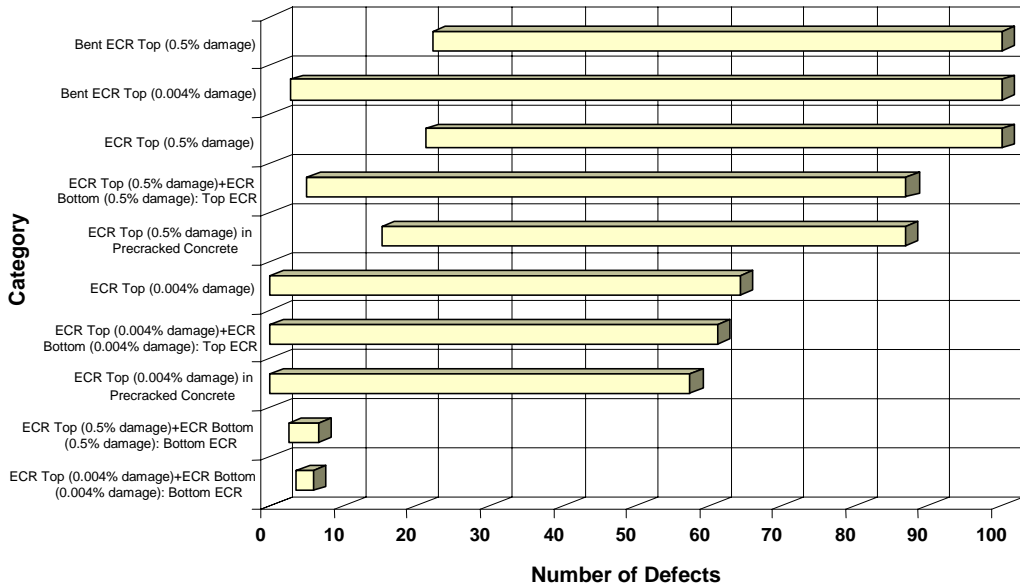
Figure 39. Ninety-five percent confidence intervals for number of final defects
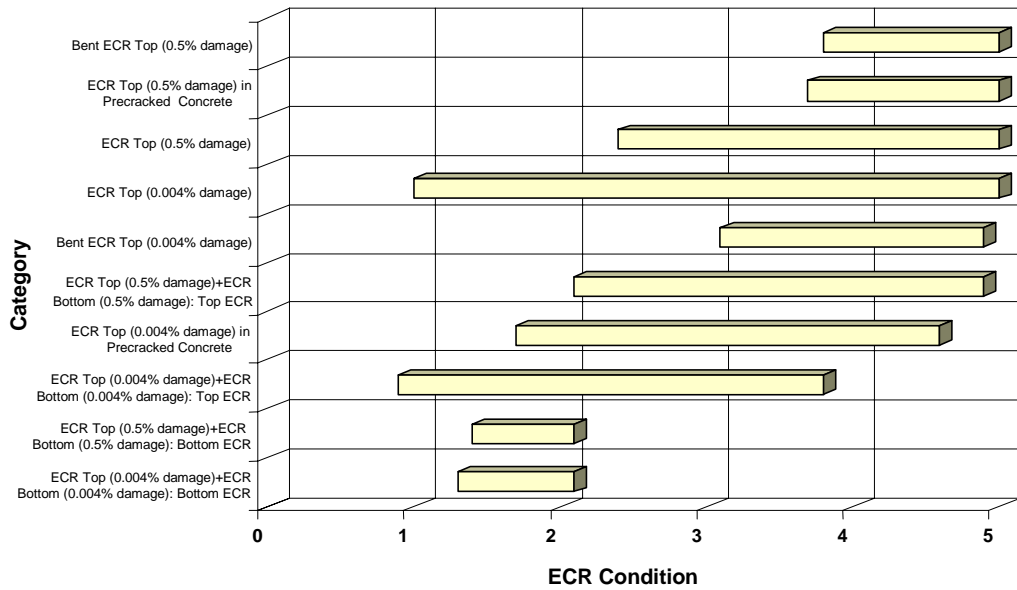
Figure 40. Ninety-five percent confidence intervals for ECR rating data
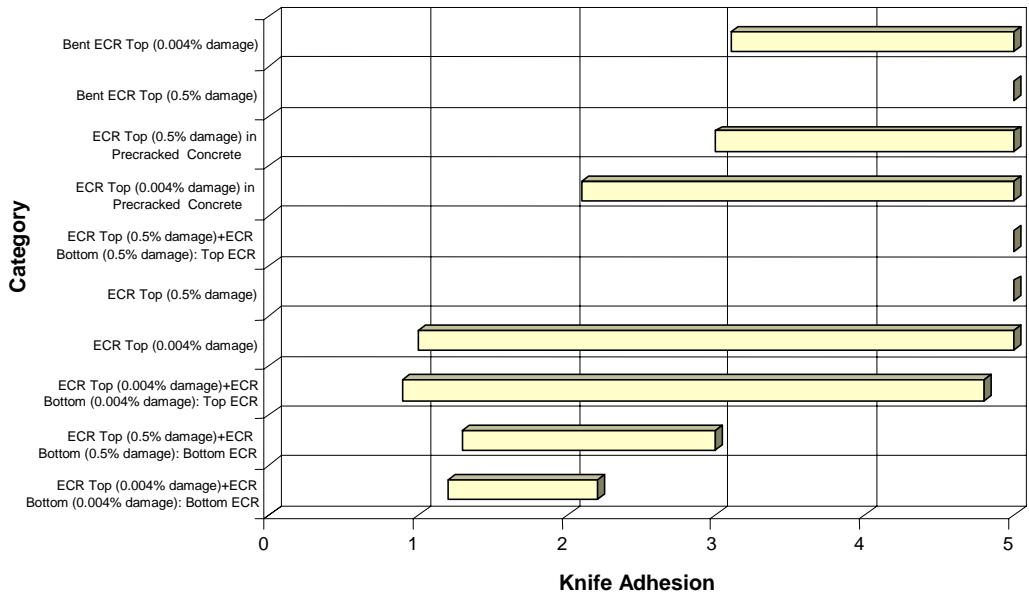
Figure 41. Ninety-five percent confidence intervals for knife adhesion data
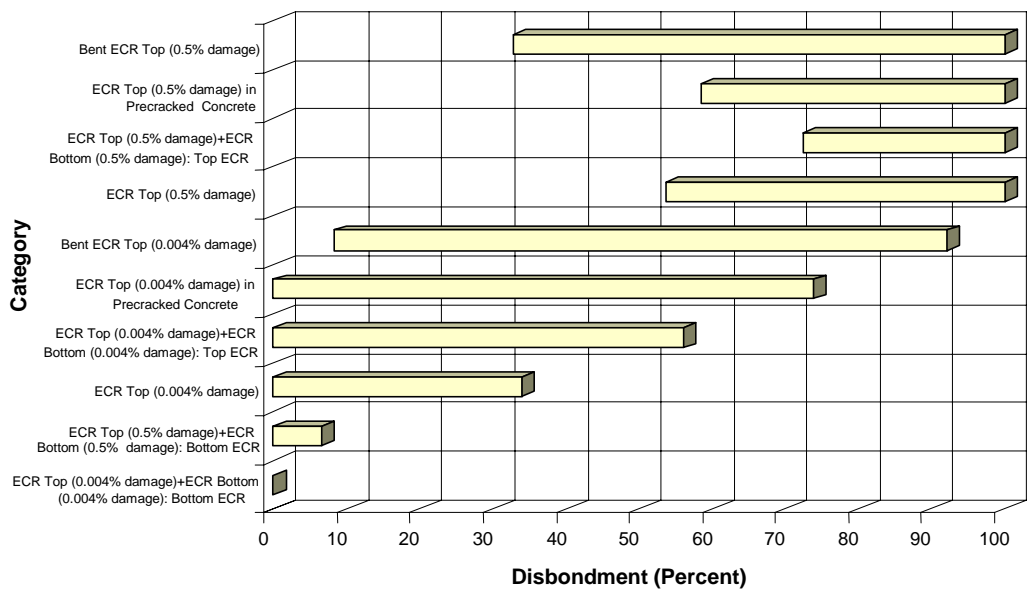
Figure 42. Ninety-five percent confidence intervals for extent of disbondment data
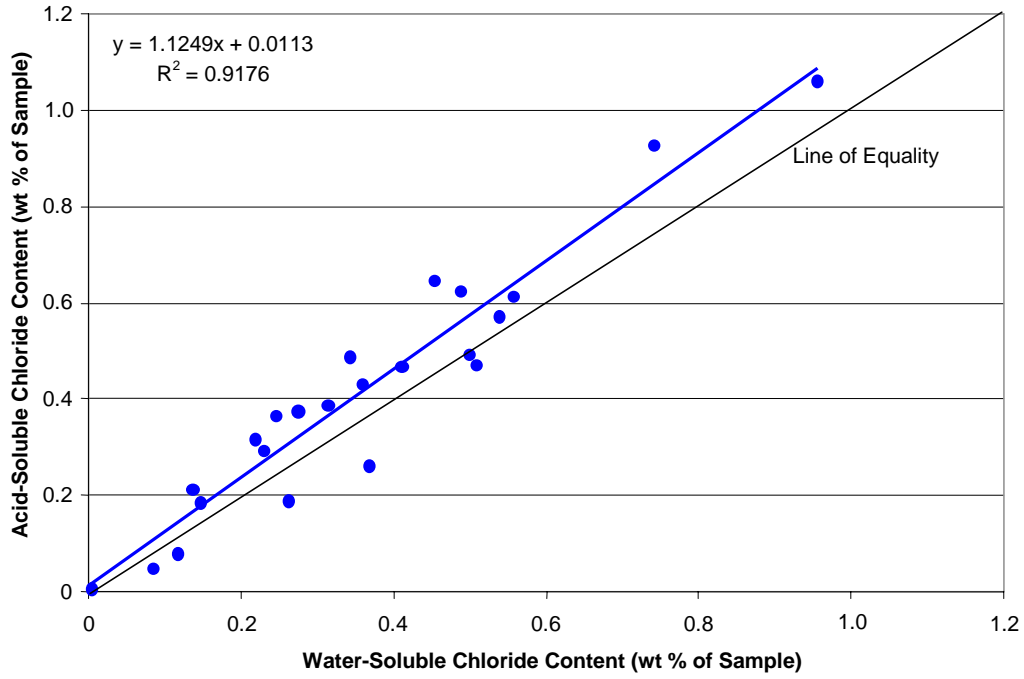
Figure 43. Relationship between water-soluble versus acid-soluble chloride data
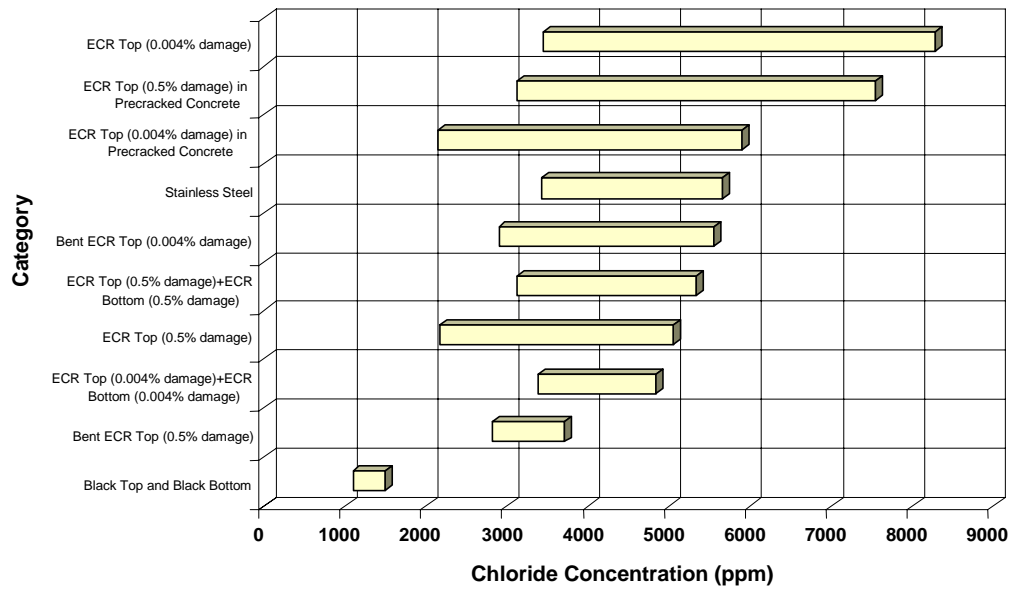
Figure 44. Ninety-five percent confidence intervals for water-soluble chloride data at top bar depth

Table 6. Electrochemical and chloride data for test slabs containing ECR in top mat only

Test Group	Slab ID	Coating Type	Top Bar ID	ECR Artificial Defect Size (Percent)	SCP (V vs. CSE)	I (uA)	OCP (V vs. CSE)	AC Resistance (Ohm)	Impedance at 0.1 Hz (Ohm)	Top Mat Water-Soluble	Top Mat Acid-Soluble	Bottom Mat Water-Soluble	Bottom Mat Acid-Soluble
Straight ECR Top + Black Bottom Uncracked Concrete.	3	C	3A	0.5	-0.403	114.1	-0.430	1.6E+02	5.1E+01	1,880			
			3B	0.004	-0.576	132.8	-0.635	2.8E+02	2.1E+02	4,300			
	6	B	6A	0.5	-0.239	67.6	-0.320	4.4E+02	3.0E+02	3,590			
			6B	0.004	-0.125	0.023	-0.308	3.2E+05	1.3E+06	4,880			
	15	D	15A	0.004	-0.064	0.0003	-0.166	2.2E+05	2.1E+06	3,660			
			15B	0.5	-0.136	0.339	-0.155	3.7E+03	1.6E+04	3,800			
	18	F	18A	0.5	-0.429	157.4	-0.479	1.8E+02	1.9E+03	5,830			
			18B	0.004	-0.489	26.9	-0.583	1.1E+03	1.0E+02	9,190			
	24	A	24A	0.5	-0.228	17.8	-0.396	2.2E+03	4.3E+03	4,100	4,690		
			24B	0.004	-0.161	0.002	-0.140	6.8E+05	1.2E+07	4,810			
	28	E	28A	0.004	-0.360	234.8	-0.597	5.2E+02	1.7E+03	8,330			
			28B	0.5	-0.392	8.5	-0.454	7.4E+02	1.9E+03	2,480			
Straight ECR Top + Black Bottom in precracked Concrete	7	A	7A	0.5	-0.384	-5.6	-0.443	2.1E+03	3.3E+03	4,080		1,680	
			7B	0.004	-0.335	-0.224	-0.399	1.4E+05	2.2E+06	2,570			
	13	C	13A	0.5	-0.174	1.2	-0.240	3.8E+03	2.8E+04	3,900			
			13B	0.004	-0.082	0.003	-0.152	1.9E+05	5.7E+05	2,400			
	14	E	14A	0.004	-0.334	0.518	-0.474	3.0E+04	1.4E+05	5,270			
			14B	0.5	-0.337	13.5	-0.396	5.5E+02	6.1E+02	5,350			
	19	F	19A	0.004	-0.471	23.8	-0.502	4.6E+02	1.2E+03	8,060			
			19B	0.5	-0.520	350	-0.572	1.6E+02	7.9E+01	9,550	10,610		
	21	D	21A	0.5	-0.152	0.002	-0.233	1.2E+04	6.7E+04	2,520			
			21B	0.004	-0.140	0.678	-0.173	9.4E+04	4.3E+05	3,500			
	25	B	25A	0.004	-0.431	-0.752	-0.383	3.8E+03	4.9E+04	3,650		1,610	
			25B	0.5	-0.508	122.3	-0.555	2.0E+02	1.6E+02	7,400	9,270		
	30	C	30A	0.004	-0.489	-0.548	-0.512	2.6E+02	1.2E+02	2,740	3,750		
			30B	0.5	-0.613	-100.7	-0.573	1.2E+02	7.4E+01	4,570		4,990	4,950
Bent ECR Top + Black Bottom Uncracked Concrete.	1	D	1A	0.5	-0.157	1.3	-0.210	4.6E+03	3.6E+04	3,670	2,620		
			1B	0.004	-0.115	0.002	-0.106	5.2E+05	1.2E+06	5,090		30	
	4	C	4A	0.5	-0.467	246.5	-0.524	2.0E+02	1.0E+02	2,850			
			4B	0.004	-0.433	320.5	-0.489	1.8E+02	7.5E+01	2,740		840	490
	8	F	8A	0.004	-0.385	248.6	-0.449	2.8E+02	9.7E+01	4,920			
			8B	0.5	-0.235	50.2	-0.297	4.4E+02	2.2E+02	3,590			
	11	B	11A	0.5	-0.312	15.2	-0.403	7.0E+02	1.0E+03	3,640			
			11B	0.004	-0.150	1.0	-0.316	5.2E+03	2.8E+04	5,080	4,720		
	22	A	22A	0.004	-0.433	51.4	-0.590	1.0E+03	1.5E+03	5,040			
			22B	0.5	-0.274	18.7	-0.318	5.9E+02	1.2E+03	3,130	3,880		
	31	E	31A	0.5	-0.130	2.6	-0.213	4.2E+03	3.2E+04	2,710			
			31B	0.004	-0.146	0.0002	-0.087	> 1100000	5.7E+06	2,450	3,660		

Table 7. Electrochemical and chloride data for test slabs containing ECR in both mats

Test Group	Slab ID	Coating Type	Bar ID	ECR Artificial defect size (Percent) Top Mat	Bottom Mat	SCP (V vs. CSE)	I (uA)	OCP (V vs. CSE)	AC Resistance (Ohm)	Impedance at 0.1 Hz (Ohm)	Top Mat Water-Soluble	Top Mat Acid-Soluble	Bottom Mat Water-Soluble	Bottom Mat Acid-Soluble
Straight Top ECR + Bottom ECR in Uncracked Concrete	2	F	2A	0.004	0.004	-0.173	0.003	-0.145	8.6E+05	1.7E+06	3,490			
			2B	0.5	0.5	-0.305	-2.3	-0.264	1.5E+03	1.8E+03	3,430	4,890	5,560	6,140
	9	B	9A	0.5	0.5	-0.459	0.134	-0.418	3.8E+03	2.1E+03	4,880	6,250		
			9B	0.004	0.004	-0.459	-0.008	-0.388	3.3E+05	6.5E+04	3,720		110	
	10	A	10A	0.5	0.5	-0.181	0.009	-0.186	6.2E+03	4.9E+04	4,520	6,470		
			10B	0.004	0.004	-0.174	0.000001	-0.165	> 1.1E+06	1.7E+06	4,180		20	
	12	C	12A	0.5	0.5	-0.521	1.4	-0.561	2.6E+03	1.8E+02	3,510		< 30	70
			12B	0.004	0.004	-0.562	0.013	-0.590	1.5E+05	1.2E+02	4,300			
	17	D	17A	0.004	0.004	-0.262	-0.00004	-0.313	6.4E+05	9.8E+05	5,370	5,720	< 800	
			17B	0.5	0.5	-0.275	0.008	-0.333	8.4E+03	9.7E+04	5,870			
	29	E	29A	0.004	0.004	-0.060	0.00005	-0.075	5.6E+05	4.9E+07	3,590			
			29B	0.5	0.5	-0.389	0.146	-0.394	3.0E+03	2.7E+03	3,160			

Table 8. Electrochemical and chloride data for test slabs containing black and stainless steel bars

Test Group	Slab ID	Bar ID	Top Mat	Bent / Straight	Bottom Mat	Precrack (Yes/ No)	SCP (V vs. CSE)	I (uA)	OCP (V vs. CSE)	AC Resistance (Ohm)	Impedance at 0.1 Hz (Ohm)	Top Mat Water-Soluble	Top Mat Acid-Soluble	Bottom Mat Water-Soluble	Bottom Mat Acid-Soluble
Black Top + Black Bottom	5	5A	Black	S	Black	N	-0.284	-83.6	-0.278	2.5E+02	1.4E+03	1,470			
		5B		S		N	-0.307	-260.1	-0.320	2.4E+02	7.5E+01	1,290		2,170	3,170
	23	23A	Black	B	Black	N	-0.334	-177.2	-0.348	1.9E+02	4.6E+01	1,670			
		23B		B		N	-0.257	-225.4	-0.235	2.1E+02	6.5E+01	1,190		1,360	2,130
	20	20A	Black	S	Black	Y	-0.360	-102.9	-0.324	3.1E+02	1.7E+02	1,210		2,290	2,940
		20B		S		Y	-0.439	0.0002	-0.302	2.5E+02	1.4E+02	1,170	800		
Stainless Steel	16	16A	Stainless Steel	B	Black	N	-0.361	-6.8	-0.257	8.7E+02	8.7E+02	5,280		2,610	1,890
		16B		B		N	-0.446	-7.8	-0.243	3.9E+02	1.2E+03	4,310			
	26	26A	Stainless Steel	S	Black	N	-0.147	0.023	-0.152	5.6E+02	2.7E+01	5,770			
		26B		S		Y	-0.197	0.06	-0.183	5.2E+02	4.9E+03	3,300			
	27	27A	Stainless Steel	S	Stainless Steel	Y	-0.230	-0.005	-0.239	5.4E+02	2.6E+03	3,330			
		27B		S		N	-0.240	0.0003	-0.169	5.4E+02	1.9E+03	5,280			

Table 9. Electrochemical test data classified by bar type

Data	Material	Slab Configuration				
		Straight Top-Black Bottom—Uncracked	Straight Top-ECR Bottom—Uncracked	Straight Top-Black Bottom—Precracked	Bent Top-Black Bottom—Uncracked	Stainless Steel
Short-Circuit Potential (V vs. CSE)	**Black**	-0.413		-0.447	-0.469	
	Stainless Steel					-0.196
	ECR with 0.004% Initial Coating Damage	-0.274	-0.272	-0.353	-0.319	
	ECR with 0.5% Initial Coating Damage	-0.341	-0.456	-0.382	-0.354	
Macrocell Current Density (uA/cm^2)	**Black**	1.239		1.240	1.304	
	Stainless Steel					0.009
	ECR with 0.004% Initial Coating Damage	0.085	0.007	0.268	0.644	
	ECR with 0.5% Initial Coating Damage	0.595	0.021	0.531	0.491	

Table 10. Electrochemical test data classified by coating type

Data	Material	Slab Configuration			
		Straight Top-Black Bottom—Uncracked	Straight Top-ECR Bottom—Uncracked	Straight Top-Black Bottom—Precracked	Bent Top-Black Bottom—Uncracked
Short-Circuit Potential (V vs. SCE)	**All ECRs Combined**	-0.291	-0.372	-0.355	-0.328
	Coating A	-0.272	-0.250	-0.303	-0.377
	Coating B	-0.217	-0.415	-0.350	-0.282
	Coating C	-0.450	-0.554	-0.346	-0.430
	Coating D	-0.149	-0.293	-0.209	-0.193
	Coating E	-0.301	-0.303	-0.427	-0.211
	Coating F	-0.387	-0.288	-0.505	-0.452
Macrocell Current Density (uA/cm^2)	**All ECRs Combined**	0.350	0.014	0.399	0.568
	Coating A	0.023	0.007	0.025	0.133
	Coating B	0.253	0.009	0.461	0.279
	Coating C	0.871	0.011	0.770	1.940
	Coating D	0.016	0.039	0.025	0.024
	Coating E	0.279	0.008	0.192	0.033
	Coating F	0.595	0.011	0.547	0.996

Table 11. Characterization of autopsied ECRs tested in the top mat

Test Group	Slab ID	Coating Type	Top Bar ID	Artificial Defect Size (Percent)	Bare Area	Mashed Area	Coating Crack	Holiday	Total	Mean	STDEV	Exterior Condition (1: excellent - 5: worst)	Knife Adhesion (1: strongest - 5: weakest)	Adhesion Loss (Percent)
Straight Top ECR + Black Bottom in Uncracked Concrete	3	C	3A	0.5	7	0	100	0	100	13.9	3.5	5	5	100
			3B	0.004	0	0	100	2	100	8.4	1.8	5	5	30
	6	B	6A	0.5	2	0	100	0	100	17.4	2.9	5	5	100
			6B	0.004	0	1	0	4	5	11.6	1.3	1	1	0
	15	D	15A	0.004	0	0	0	2	2	11.8	0.5	1	1	0
			15B	0.5	2	0	0	0	2	13.0	0.8	1	5	26
	18	F	18A	0.5	7	0	100	0	100	14.6	3.1	5	5	100
			18B	0.004	3	0	16	0	19	9.1	1.4	5	5	32
	24	A	24A	0.5	2	0	16	1	19	9.4	1.8	4	5	85
			24B	0.004	4	0	0	0	4	7.6	0.6	2	2	0
	28	E	28A	0.004	0	1	18	0	19			4	5	33
			28B	0.5	3	0	100	0	100			4	5	95
Straight ECR Top + Black Bottom in precracked Concrete	7	A	7A	0.5	2	2	28	2	34	10.6	2.5	4	5	100
			7B	0.004	0	0	3	3	6	9.1	1.2	3	5	23
	13	C	13A	0.5	2	0	1	1	4	10.4	1.5	3	1	46
			13B	0.004	0	2	0	3	5	9.4	1.2	1	1	0
	14	E	14A	0.004	0	1	0	2	3	9.1	1.1	2	3	2
			14B	0.5	8	2	26	4	40	12.1	5.3	5	5	61
	19	F	19A	0.004	1	0	23	2	26	14.7	2.8	5	5	56
			19B	0.5	17	0	100	0	100	17.5	3.3	5	5	100
	21	D	21A	0.5	2	2	10	0	14	14.1	2.0	4	5	60
			21B	0.004	0	0	0	1	1	14.6	1.0	2	2	0
	25	B	25A	0.004	2	3	23	4	32	9.1	1.9	4	5	74
			25B	0.5	10	7	46	2	65	15.7	3.5	5	5	100
	30	C	30A	0.004	4	0	100	0	100	18.5	4.7	5	5	100
			30B	0.5	2	0	100	0	100	18.4	4.9	5	5	100
Bent Top ECR + Black Bottom in Uncracked Concrete	1	D	1A	0.5	3	4	0	0	7	14.3	1.2	3	5	50
			1B	0.004	1	1	0	0	2	15.4	1.3	3	2	0
	4	C	4A	0.5	6	0	100	0	100	10.7	3.3	5	5	50
			4B	0.004	5	0	100	0	100	13.0	4.3	5	5	68
	8	F	8A	0.004	13	0	100	0	100	15.5	3.5	5	5	100
			8B	0.5	3	0	100	0	100	19.7	5.6	5	5	100
	11	B	11A	0.5	4	0	61	0	65	16.0	3.3	5	5	100
			11B	0.004	0	1	4	6	11	10.9	1.5	3	5	56
	22	A	22A	0.004	0	2	100	0	100	10.3	1.1	4	5	73
			22B	0.5	5	0	100	0	100	11.4	1.9	5	5	100
	31	E	31A	0.5	11	9	2	2	24	7.1	1.7	5	5	18
			31B	0.004	7	5	2	2	16	7.2	1.9	4	4	4

Table 12. Characterization of autopsied ECRs tested in both mats

Test Group	Slab ID	Coating Type	Bar ID	Artificial Defect Size (Percent)	Number of Final Defects					Coating Thickness (mils)		Exterior Condition (1: excellent - 5: worst)	Knife Adhesion (1: strongest - 5: weakest)	Adhesion Loss (Percent)
					Bare Area	Mashed Area	Coating Crack	Holiday	Total	Mean	STDEV			
Straight ECR Top + Bottom ECR in Uncracked Concrete	2	F	2A-Top	0.004	2	0	1	0	3	10.6	1.8	2	3	3
			2B-Top	0.5	8	0	71	2	81	13.2	2.5	5	5	100
			2A-Bottom 1	0.004	3	0	1	2	6	9.2	3.0	1	3	0
			2A-Bottom 2	0.004	7	1	0	1	9	13.3	2.0	1	2	0
			2B-Bottom 1	0.5	2	2	1	0	5	9.3	0.6	1	5	22
			2B-Bottom 2	0.5	8	2	2	0	12	8.2	0.9	2	4	5
	9	B	9A-Top	0.5	2	0	39	4	45	11.5	1.6	3	5	96
			9B-Top	0.004	0	0	0	3	3	9.7	1.0	2	5	19
			9A-Bottom 1	0.5	2	0	0	0	2	10.9	1.0	1	1	0
			9A-Bottom 2	0.5	0	0	0	4	4	10.4	0.6	2	1	0
			9B-Bottom 1	0.004	0	2	1	2	5	10.4	0.7	1	1	0
			9B-Bottom 2	0.004	2	0	0	0	2	10.7	0.7	1	1	0
	10	A	10A-Top	0.5	3	0	4	0	7	8.8	1.1	2	5	61
			10B-Top	0.004	0	4	0	4	8	7.9	0.9	2	1	0
			10A-Bottom 1	0.5	2	0	0	0	2	7.5	0.8	1	2	0
			10A-Bottom 2	0.5	2	0	0	0	2	8.2	1.0	2	3	0
			10B-Bottom 1	0.004	2	1	0	4	7	8.3	0.8	3	1	0
			10B-Bottom 2	0.004	0	0	0	4	4	8.2	0.7	2	3	0
	12	C	12A-Top	0.5	7	3	100	0	100	9.7	2.4	5	5	90
			12B-Top	0.004	9	0	100	0	100	9.7	2.4	5	5	90
			12A-Bottom 1	0.5	2	1	0	0	3	8.3	1.1	1	1	0
			12A-Bottom 2	0.5	1	6	2	0	9	8.2	1.0	3	2	0
			12B-Bottom 1	0.004	0	0	0	4	4	8.7	2.4	1	1	0
			12B-Bottom 2	0.004	0	0	0	3	3	8.5	0.8	2	2	0
	17	D	17A-Top	0.004	1	0	0	1	2	12.8	0.9	2	2	0
			17B-Top	0.5	2	0	0	0	2	13.0	0.8	2	5	13
			17A-Bottom 1	0.004	0	0	0	4	4	14.5	1.0	2	1	0
			17A-Bottom 2	0.004	0	0	0	4	4	13.7	0.8	2	2	0
			17B-Bottom 1	0.5	2	0	0	0	2	14.3	0.9	2	1	0
			17B-Bottom 2	0.5	2	0	0	1	3	13.1	1.1	2	2	0
	29	E	29A-Top	0.004	0	0	0	3	3	8.4	1.9	1	1	0
			29B-Top	0.5	6	2	32	1	41	7.9	0.9	4	5	75
			29A-Bottom 1	0.004	1	0	0	4	5	8.1	0.9	2	2	0
			29A-Bottom 2	0.004	4	0	0	0	4	9.9	1.3	2	1	0
			29B-Bottom 1	0.5	3	0	0	0	3	8.9	0.8	2	1	0
			29B-Bottom 2	0.5	2	5	0	0	7	7.9	1.0	2	3	4

CHAPTER 4. CONCLUSIONS

1. The black bars produced the highest mean macrocell current density among various combinations of test variables regardless of slab configuration, i.e., presence of crack and bar shape (bent vs. straight). The highest mean macrocell current density (1.3 µA/cm^2 (8.4 µA/inch^2)) was obtained from the black bent bar coupled with black bottom bars in uncracked concrete. In contrast, the stainless steel bars exhibited negligible mean macrocell current density, which was only 1 percent of the highest black bar case. Autopsy revealed that the corrosion morphology of black and stainless steel bars was consistent with the macrocell current density data. Macrocell current density was a good performance indicator of test slabs.

2. For straight top mat ECRs, the mean macrocell current density was influenced by the size of initial coating damage and type of bar in the bottom mat. When they were coupled with black bars in the bottom mat, the size of the coating defect became a critical factor for controlling macrocell current density. In the case of straight top mat ECRs containing 0.004 percent of initial coating defect coupled with black bottom bars, the mean macrocell current density was 7 to 21 percent of the highest black bar case, depending on whether the slab was precracked. If straight top mat ECRs containing 0.5 percent coating damage were connected to the black bottom bars, the current values increased to more than 40 percent of the black bar value, regardless of precracks in the concrete.

3. However, if straight ECRs in the top mat were connected to ECRs in the bottom mat in uncracked concrete, the mean macrocell current density decreased to no greater than 2 percent of the highest black bar case, regardless of the initial coating defect size. They behaved comparable to stainless steel bars.

4. For bent ECRs, even ones containing 0.004 percent coating damage produced noticeable macrocell current density when they were connected to black bottom bars, such that mean macrocell current density increased to 38 and 49 percent of the highest black bar case, regardless of initial coating defect size. In general, bent ECRs coupled with black bottom bars performed the worst of the ECR cases.

5. Mean macrocell current density varied significantly by coating type; this could be related to coating quality. However, when ECRs were used in both mats, such variation disappeared, and all bars behaved very well with very low mean macrocell current density.

6. The SCP data obtained during this test program exhibited large data scatter with time, and no consistent trends developed that could lead to compare the corrosion performance of different bar types and shapes.

7. Whenever an ECR slab with negligible macrocell current density was autopsied, the appearance of the ECR and concrete/bar interface was excellent with no sign of corrosion, and the coating looked new with a glossy texture. However, when severely corroded ECRs recognized by high macrocell current densities were autopsied, they revealed coating

deterioration due to corrosion and exhibited numerous hairline cracks and/or blisters in conjunction with extensive coating disbondment and underlying steel corrosion. When test slabs exhibited severe damage, electrochemical test data collected from those slabs did not provide meaningful results.

8. Final defects were classified as bare area, mashed area (mechanical damage), coating crack, and holiday. Generally, the number of final coating defects on the autopsied ECRs increased from their initial values determined before embedment in concrete. This phenomenon was particularly pronounced for the poorly performing bars due to development of coating cracks, which was the most frequent form of coating deterioration. Accumulation of multiple rust layers beneath disbonded coating is also a common corrosion morphology observed on severely corroded ECRs.

9. Reduced adhesion was usually initiated at the initial coating defects. It was much more pronounced on the top mat ECRs, irrespective of whether they were removed from ECR top-black bottom slabs or the ECR top-ECR bottom slabs, compared to those extracted from the bottom mat. The ECRs removed from the bottom mat also exhibited the lowest number of final defects and the strongest knife adhesion. No consistent trend was found between the level of macrocell current density and the extent of adhesion loss. Earlier FHWA studies investigated the coatings' adhesion using solution immersion tests and cathodic disbonding tests.[2,4] Based on the review of the test results, the adhesion, as tested by solution immersion and cathodic disbonding tests, appeared to be a poor indicator of long-term performance of the coated bars in concrete. These findings suggest that there is no direct relationship between loss of adhesion and the effectiveness of ECR to mitigate corrosion.

10. According to impedance modulus, AC resistance, macrocell current density data, and autopsy results, the excellent performance of test slabs containing ECRs in both mats comparable to stainless steel bars may be attributed to the facts that electrical resistance was very high between the two ECR mats, and the ECRs in the bottom mat suppress the corrosion activity at the top mat ECR by minimizing the size of the available cathode.

11. This 7-year laboratory and outdoor exposure study confirmed that using ECRs in the top mat of simulated bridge decks can reduce the corrosion susceptibility to at least 50 percent of the black bar case, even when ECR with poor coating condition is used. If ECRs are used in both mats in uncracked concrete, this corrosion resistance can increase dramatically, and can approach the corrosion-resistant level of stainless steel reinforcement. This conclusion is valid even when they contain coating defects.

REFERENCES

1.   McDonald, D.B., Sherman, M.R., and Pfeifer, D.W., *The Performance of Bendable and Nonbendable Organic Coatings for Reinforcing Bars in Solution and Cathodic Debonding Tests*, Report No. FHWA-RD-94-103, Federal Highway Administration, McLean, VA, January 1995, 148 pp.

2.   McDonald, D.B., Sherman, M.R., and Pfeifer, D.W., *The Performance of Bendable and Nonbendable Organic Coatings for Reinforcing Bars in Solution and Cathodic Debonding Tests: Phase II Screening Tests*, Report No. FHWA-RD-96-021, Federal Highway Administration, McLean, VA, May 1996, 121 pp.

3.   McDonald, D.B., Pfeifer, D.W., and Blake, G.T., *The Corrosion Performance of Inorganic-, Ceramic-, and Metallic-Clad Reinforcing Bars and Solid Metallic Reinforcing Bars in Accelerated Screening Tests*, Report No. FHWA-RD-96-085, Federal Highway Administration, McLean, VA, October 1996, 112 pp.

4.   McDonald, D.B., Pfeifer, D.W., and Sherman, M.R., *Corrosion Evaluation of Epoxy-Coated, Metallic-Clad, and Solid Metallic Reinforcing Bars in Concrete*, Report No. FHWA-RD-98-153, Federal Highway Administration, McLean, VA, December 1998, 137 pp.

b) Rear view

Specimen ID	1A	1B
Top mat	Coating D	Coating D
Bar shape (straight/bent)	Bent	Bent
Coating defect (%)	0.5	0.004
Bottom mat	Black	
Coating defect (%)	N/A	N/A
Precracked	No	No

d) Slab specifications

a) Front view

c) Top view

Figure 45. Slab #1 front, rear, and top views with specifications
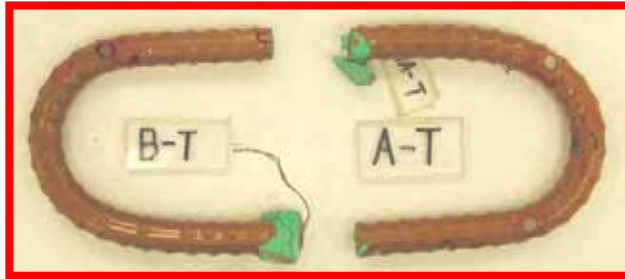
a) Top bars

b) Bottom bars

*__A-T__: Top left bar, __B-T__: Top right bar, __A-B1&B2__: Bottom left bars, __B-B1&B2__: Bottom right bars

Figure 46. Slab #1 extracted rebars condition

a) Top bars

b) Bottom bars

***A-T**: Top left bar, **B-T**: Top right bar, **A-B1&B2**: Bottom left bars, **B-B1&B2**: Bottom right bars

Figure 47. Slab #1 after autopsy

a) Front view

b) Rear view

c) Top view

Specimen ID	2A	2B
Top mat	Coating F	Coating F
Bar shape (straight/bent)	Straight	Straight
Coating defect (%)	0.004	0.5
Bottom mat	Coating F	
Coating defect (%)	0.004	0.5
Precracked	No	No

d) Slab specifications

Figure 48. Slab #2 front, rear, and top views with specifications
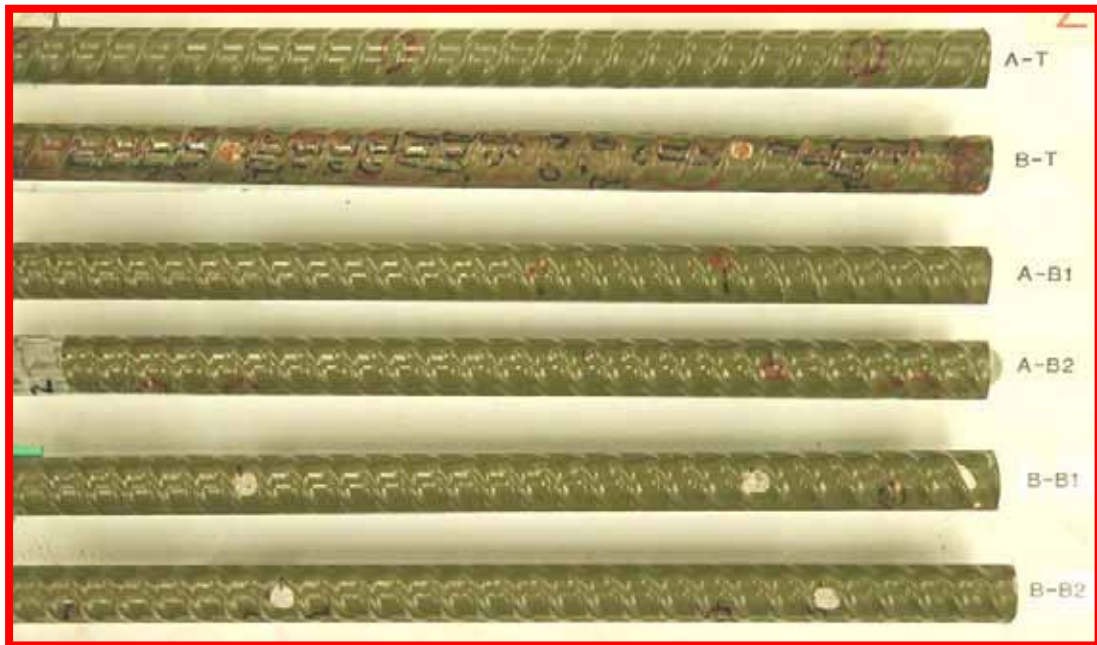
Figure 49. Slab #2 extracted rebars condition

Figure 50. Slab #2 after autopsy

***A-T**: Top left bar, **B-T**: Top right bar, **A-B1&B2**: Bottom left bars, **B-B1&B2**: Bottom right bars

b) Rear view

a) Front view

c) Top view

Specimen ID	3A	3B
Top mat	Coating C	Coating C
Bar shape (straight/bent)	Straight	Straight
Coating defect (%)	0.5	0.004
Bottom mat	Black	
Coating defect (%)	N/A	N/A
Precracked	No	No

d) Slab specifications

Figure 51. Slab #3 front, rear, and top views with specifications

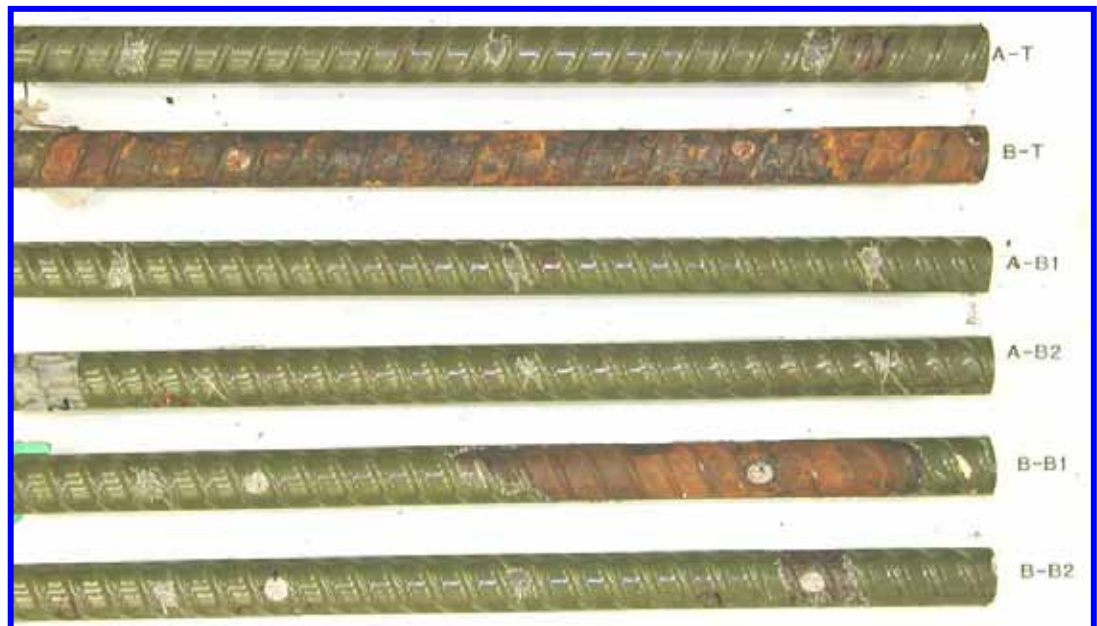Figure 52. Slab #3 extracted rebars condition

Figure 53. Slab #3 after autopsy

***A-T**: Top left bar, **B-T**: Top right bar, **A-B1&B2**: Bottom left bars, **B-B1&B2**: Bottom right bars

b) Rear view

Specimen ID	4A	4B
Top mat	Coating C	Coating C
Bar shape (straight/bent)	Bent	Bent
Coating defect (%)	0.5	0.004
Bottom mat	Black	
Coating defect (%)	N/A	N/A
Precracked	No	No

d) Slab specifications

a) Front view

c) Top view

Figure 54. Slab #4 front, rear, and top views with specifications

58

a) Top bars

b) Bottom bars

***A-T**: Top left bar, **B-T**: Top right bar, **A-B1&B2**: Bottom left bars, **B-B1&B2**: Bottom right bars

Figure 55. Slab #4 extracted rebars condition

a) Top bars

b) Bottom bars

*__A-T__: Top left bar, __B-T__: Top right bar, __A-B1&B2__: Bottom left bars, __B-B1&B2__: Bottom right bars

Figure 56. Slab #4 after autopsy

b) Rear view

Specimen ID	5A	5B
Top mat	Black	Black
Bar shape (straight/bent)	Straight	Straight
Coating defect (%)	N/A	N/A
Bottom mat	Black	
Coating defect (%)	N/A	N/A
Precracked	No	No

d) Slab specifications

a) Front view

c) Top view

Figure 57. Slab #5 front, rear, and top views with specifications

Figure 58. Slab #5 extracted rebars condition

Figure 59. Slab #5 after autopsy

***A-T**: Top left bar, **B-T**: Top right bar, **A-B1&B2**: Bottom left bars, **B-B1&B2**: Bottom right bars

b) Rear view

a) Front view

c) Top view

Specimen ID	6A	6B
Top mat	Coating B	Coating B
Bar shape (straight/bent)	Straight	Straight
Coating defect (%)	0.5	0.004
Bottom mat	Black	
Coating defect (%)	N/A	N/A
Precracked	No	No

d) Slab specifications

Figure 60. Slab #6 front, rear, and top views with specifications
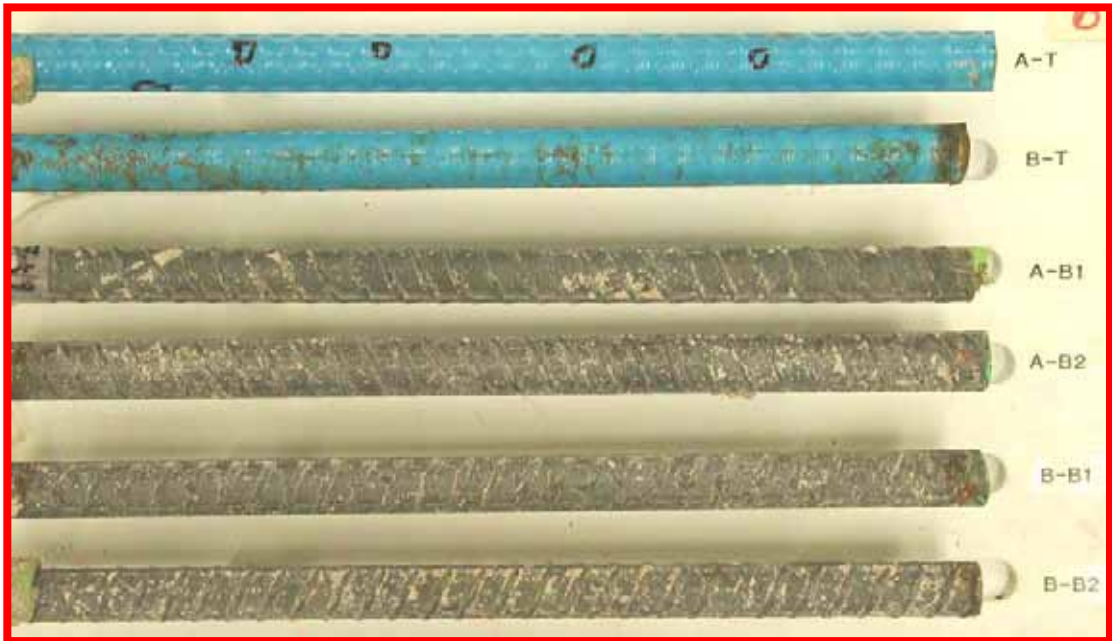
Figure 61. Slab #6 extracted rebars condition

Figure 62. Slab #6 after autopsy

***A-T**: Top left bar, **B-T**: Top right bar, **A-B1&B2**: Bottom left bars, **B-B1&B2**: Bottom right bars

b) Rear view

Specimen ID	7A	7B
Top mat	Coating A	Coating A
Bar shape (straight/bent)	Straight	Straight
Coating defect (%)	0.5	0.004
Bottom mat	Black	
Coating defect (%)	N/A	N/A
Precracked	Yes	Yes

d) Slab specifications

a) Front view

c) Top view

Figure 63. Slab #7 front, rear, and top views with specifications
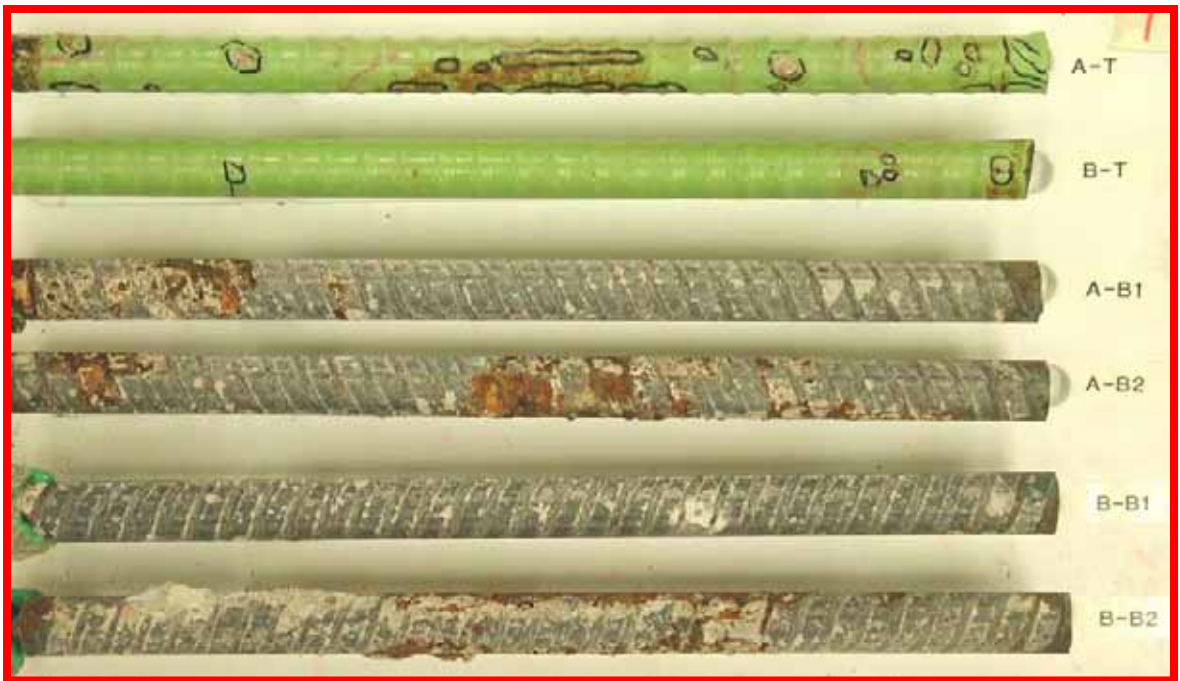
Figure 64. Slab #7 extracted rebars condition

Figure 65. Slab #7 after autopsy

***A-T**: Top left bar, **B-T**: Top right bar, **A-B1&B2**: Bottom left bars, **B-B1&B2**: Bottom right bars

b) Rear view

Specimen ID	8A	8B
Top mat	Coating F	Coating F
Bar shape (straight/bent)	Bent	Bent
Coating defect (%)	0.004	0.5
Bottom mat	Black	
Coating defect (%)	N/A	N/A
Precracked	No	No

d) Slab specifications

a) Front view

c) Top view

Figure 66. Slab #8 front, rear, and top views with specifications
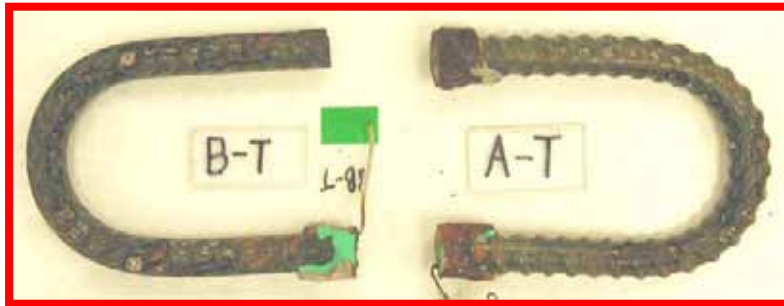
67

a) Top bars

b) Bottom bars

*__A-T__: Top left bar, __B-T__: Top right bar, __A-B1&B2__: Bottom left bars, __B-B1&B2__: Bottom right bars

Figure 67. Slab #8 extracted rebars condition

a) Top bars

b) Bottom bars

*__A-T__: Top left bar, __B-T__: Top right bar, __A-B1&B2__: Bottom left bars, __B-B1&B2__: Bottom right bars

Figure 68. Slab #8 after autopsy

b) Rear view

a) Front view

c) Top view

Specimen ID	9A	9B
Top mat	Coating B	Coating B
Bar shape (straight/bent)	Straight	Straight
Coating defect (%)	0.5	0.004
Bottom mat	Coating B	
Coating defect (%)	0.5	0.004
Precracked	No	No

d) Slab specifications

Figure 69. Slab #9 front, rear, and top views with specifications
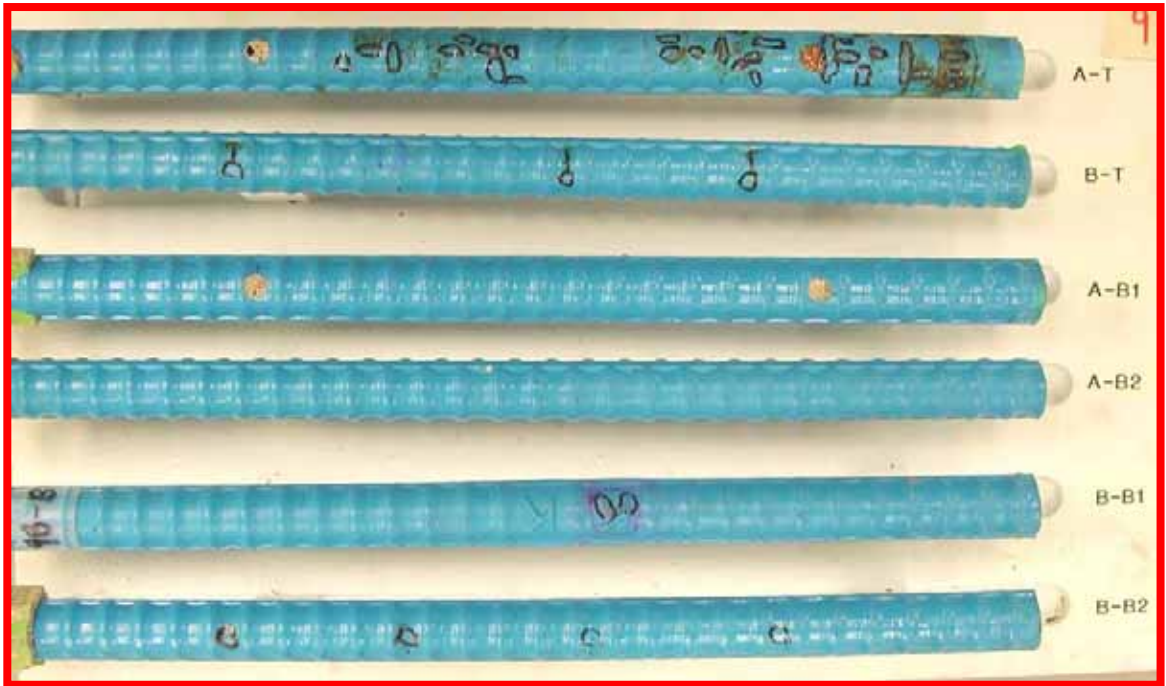
Figure 70. Slab #9 extracted rebars condition

Figure 71. Slab #9 after autopsy

***A-T**: Top left bar, **B-T**: Top right bar, **A-B1&B2**: Bottom left bars, **B-B1&B2**: Bottom right bars
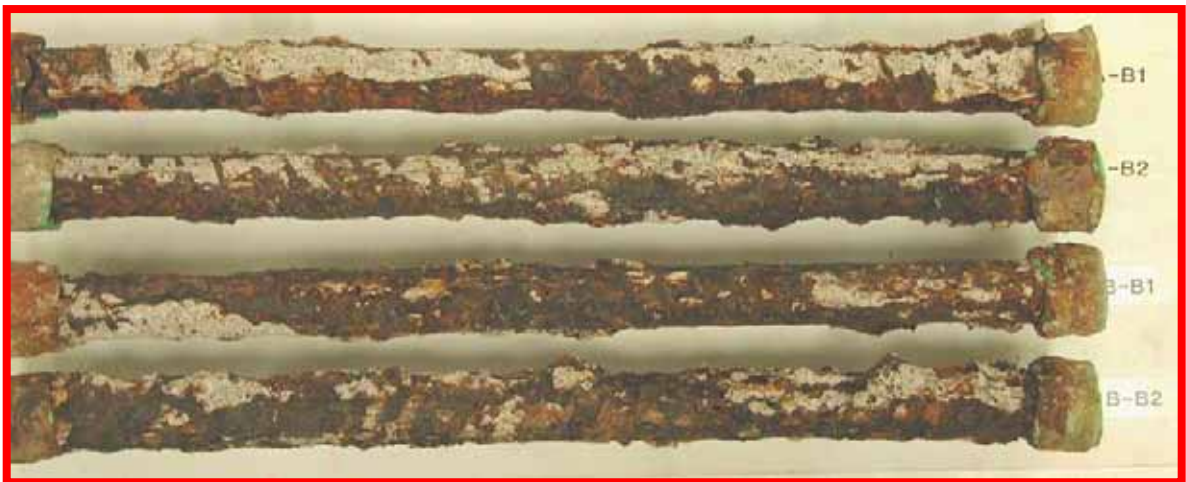
b) Rear view

a) Front view

c) Top view

Specimen ID	10A	10B
Top mat	Coating A	Coating A
Bar shape (straight/bent)	Straight	Straight
Coating defect (%)	0.5	0.004
Bottom mat	Coating A	
Coating defect (%)	0.5	0.004
Precracked	No	No

d) Slab specifications

Figure 72. Slab #10 front, rear, and top views with specifications
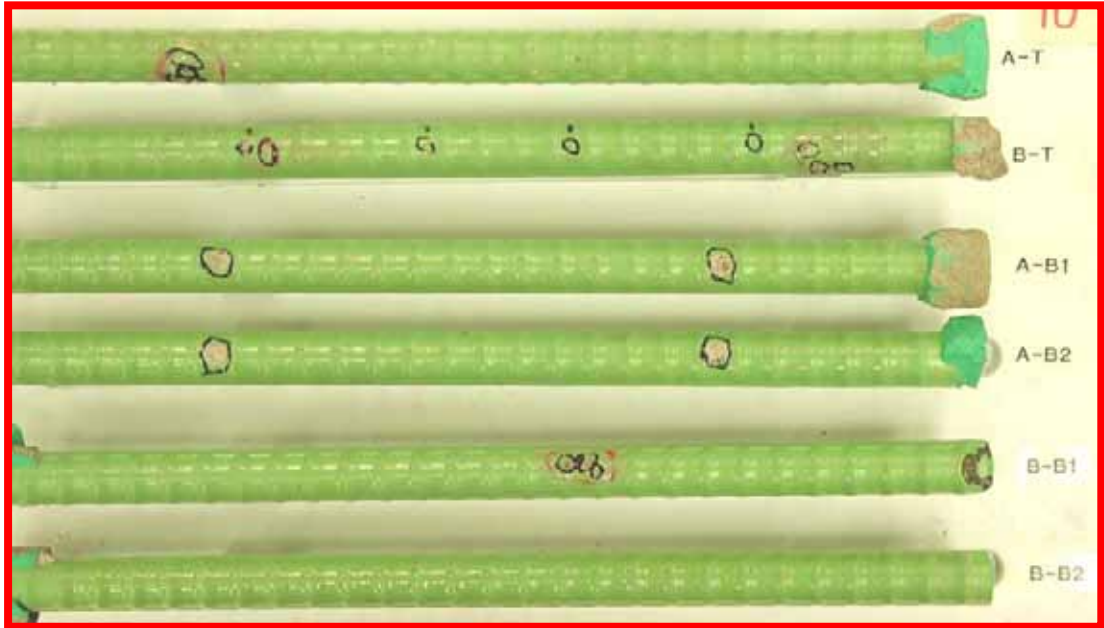
Figure 73. Slab #10 extracted rebars condition

Figure 74. Slab #10 after autopsy

***A-T**: Top left bar, **B-T**: Top right bar, **A-B1&B2**: Bottom left bars, **B-B1&B2**: Bottom right bars

b) Rear view

a) Front view

c) Top view

Specimen ID	11A	11B
Top mat	Coating B	Coating B
Bar shape (straight/bent)	Bent	Bent
Coating defect (%)	0.5	0.004
Bottom mat	Black	
Coating defect (%)	N/A	N/A
Precracked	No	No

d) Slab specifications

Figure 75. Slab #11 front, rear, and top views with specifications
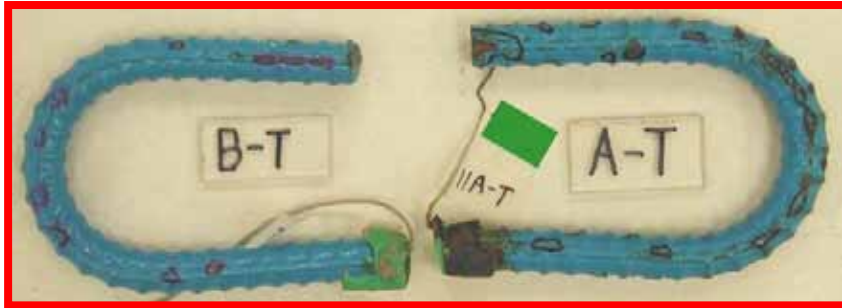
74

a) Top bars

b) Bottom bars

***A-T**: Top left bar, **B-T**: Top right bar, **A-B1&B2**: Bottom left bars, **B-B1&B2**: Bottom right bars

Figure 76. Slab #11 extracted rebars condition

a) Top bars

b) Bottom bars

*__A-T__: Top left bar, __B-T__: Top right bar, __A-B1&B2__: Bottom left bars, __B-B1&B2__: Bottom right bars

Figure 77. Slab #11 after autopsy

b) Rear view

Specimen ID	12A	12B
Top mat	Coating C	Coating C
Bar shape (straight/bent)	Straight	Straight
Coating defect (%)	0.5	0.004
Bottom mat	Coating C	
Coating defect (%)	0.5	0.004
Precracked	No	No

d) Slab specifications

a) Front view

c) Top view

Figure 78. Slab #12 front, rear, and top views with specifications
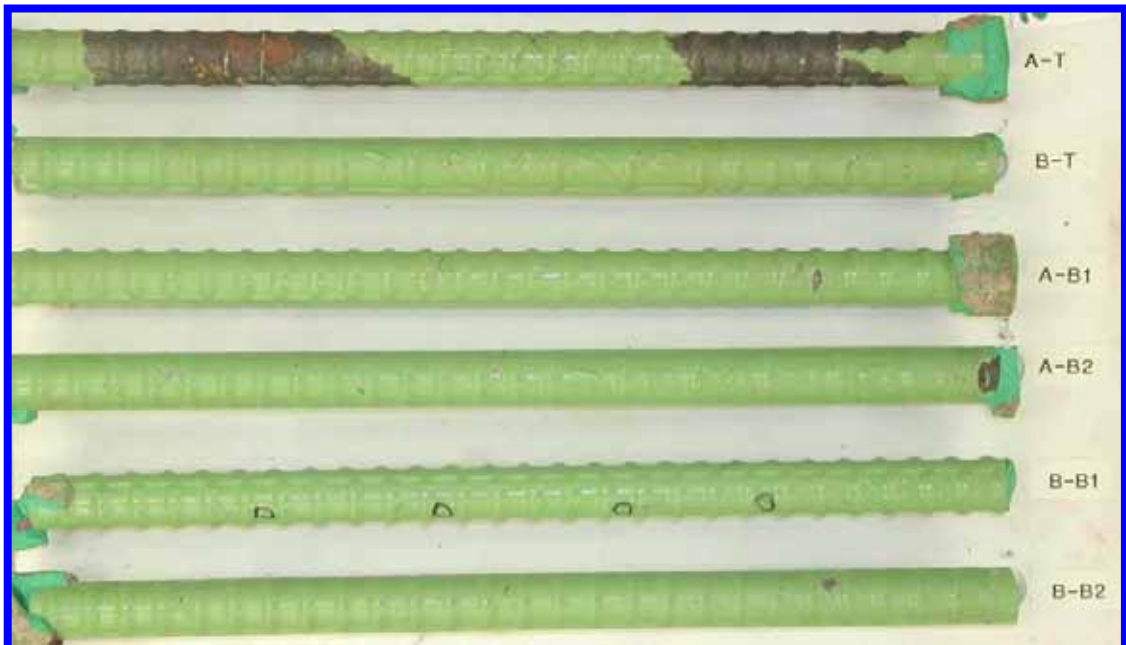
Figure 79. Slab #12 extracted rebars condition

Figure 80. Slab #12 after autopsy

***A-T**: Top left bar, **B-T**: Top right bar, **A-B1&B2**: Bottom left bars, **B-B1&B2**: Bottom right bars

b) Rear view

| Specimen ID	13A	13B
Top mat	Coating C	Coating C
Bar shape (straight/bent)	Straight	Straight
Coating defect (%)	0.5	0.004
Bottom mat		Black
Coating defect (%)	N/A	N/A
Precracked	Yes	Yes

d) Slab specifications

a) Front view

c) Top view

Figure 81. Slab #13 front, rear, and top views with specifications

Figure 82. Slab #13 extracted rebars condition

Figure 83. Slab #13 after autopsy

***A-T**: Top left bar, **B-T**: Top right bar, **A-B1&B2**: Bottom left bars, **B-B1&B2**: Bottom right bars

b) Rear view

a) Front view

c) Top view

Specimen ID	14A	14B
Top mat	Coating E	Coating E
Bar shape (straight/bent)	Straight	Straight
Coating defect (%)	0.004	0.5
Bottom mat	Black	
Coating defect (%)	N/A	N/A
Precracked	Yes	Yes

d) Slab specifications

Figure 84. Slab #14 front, rear, and top views with specifications
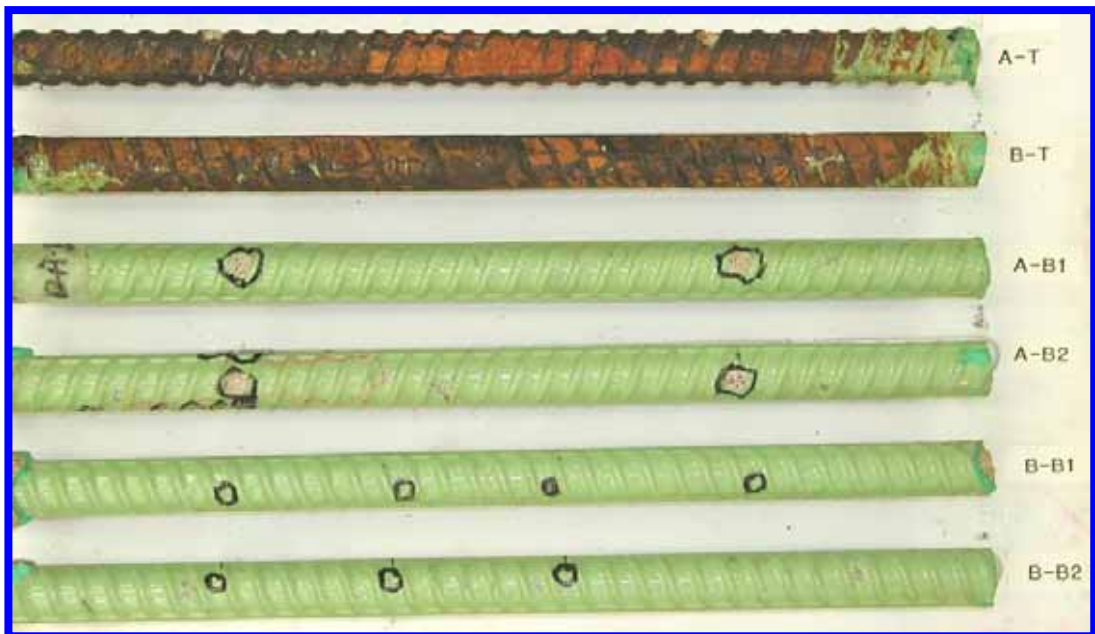
81
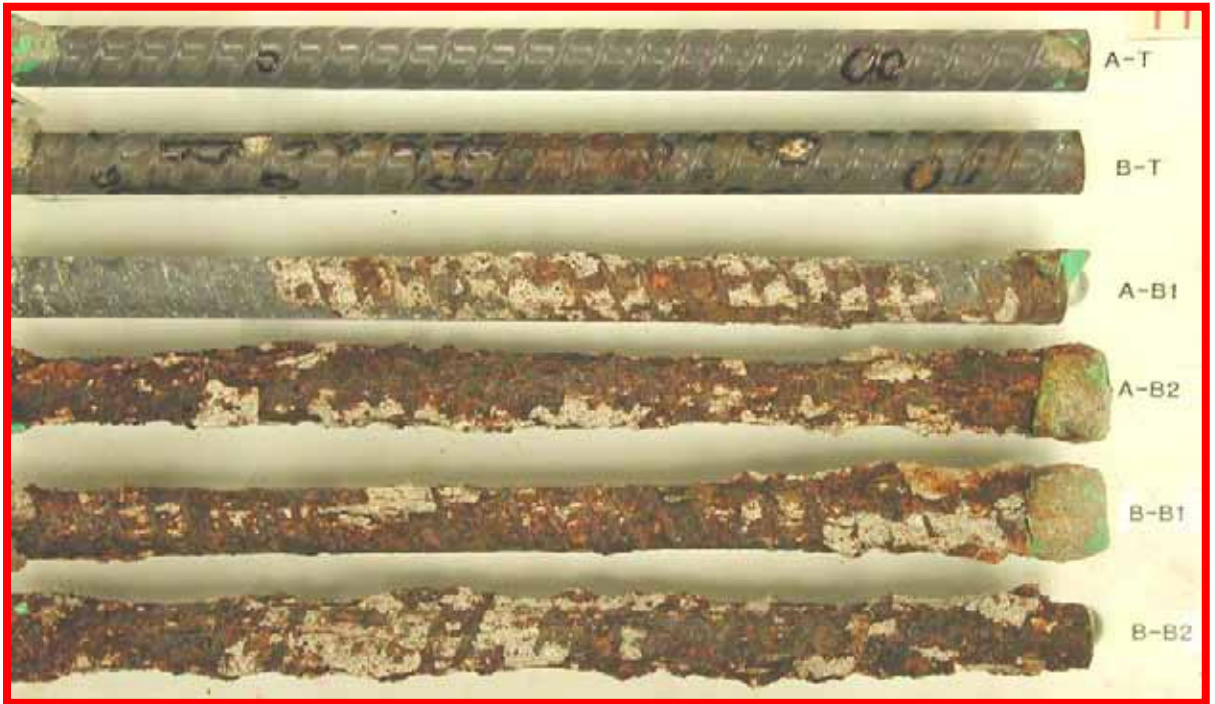
Figure 85. Slab #14 extracted rebars condition

Figure 86. Slab #14 after autopsy

***A-T**: Top left bar, **B-T**: Top right bar, **A-B1&B2**: Bottom left bars, **B-B1&B2**: Bottom right bars

b) Rear view

a) Front view

c) Top view

Specimen ID	15A	15B
Top mat	Coating D	Coating D
Bar shape (straight/bent)	Straight	Straight
Coating defect (%)	0.004	0.5
Bottom mat	Black	
Coating defect (%)	N/A	N/A
Precracked	No	No

d) Slab specifications

Figure 87. Slab #15 front, rear, and top views with specifications

Figure 88. Slab #15 extracted rebars condition

Figure 89. Slab #15 after autopsy

***A-T**: Top left bar, **B-T**: Top right bar, **A-B1&B2**: Bottom left bars, **B-B1&B2**: Bottom right bars

b) Rear view

a) Front view

Specimen ID	16A	16B
Top mat	Stainless Steel	Stainless Steel
Bar shape (straight/bent)	Bent	Bent
Coating defect (%)	N/A	N/A
Bottom mat	Black	
Coating defect (%)	N/A	N/A
Precracked	No	No

d) Slab specifications

c) Top view

Figure 90. Slab #16 front, rear, and top views with specifications

a) Top bars

b) Bottom bars

***A-T**: Top left bar, **B-T**: Top right bar, **A-B1&B2**: Bottom left bars, **B-B1&B2**: Bottom right bars

Figure 91. Slab #16 extracted rebars condition

a) Top bars

b) Bottom bars

*A-T: Top left bar, **B-T**: Top right bar, **A-B1&B2**: Bottom left bars, **B-B1&B2**: Bottom right bars

Figure 92. Slab #16 after autopsy

b) Rear view

a) Front view

c) Top view

Specimen ID	17A	17B
Top mat	Coating D	Coating D
Bar shape (straight/bent)	Straight	Straight
Coating defect (%)	0.004	0.5
Bottom mat	Coating D	
Coating defect (%)	0.004	0.5
Precracked	No	No

d) Slab specifications

Figure 93. Slab #17 front, rear, and top views with specifications

Figure 94. Slab #17 extracted rebars condition

Figure 95. Slab #17 after autopsy

*A-T: Top left bar, B-T: Top right bar, A-B1&B2: Bottom left bars, B-B1&B2: Bottom right bars

b) Rear view

a) Front view

Specimen ID	18A	18B
Top mat	Coating F	Coating F
Bar shape (straight/bent)	Straight	Straight
Coating defect (%)	0.5	0.004
Bottom mat	Black	
Coating defect (%)	N/A	N/A
Precracked	No	No

d) Slab specifications

c) Top view

Figure 96. Slab #18 front, rear, and top views with specifications

Figure 97. Slab #18 extracted rebars condition

Figure 98. Slab #18 after autopsy

*A-T: Top left bar, B-T: Top right bar, A-B1&B2: Bottom left bars, B-B1&B2: Bottom right bars

b) Rear view

a) Front view

Specimen ID	19A	19B
Top mat	Coating F	Coating F
Bar shape (straight/bent)	Straight	Straight
Coating defect (%)	0.004	0.5
Bottom mat		Black	
Coating defect (%)	N/A	N/A
Precracked	Yes	Yes

d) Slab specifications

c) Top view

Figure 99. Slab #19 front, rear, and top views with specifications

92

Figure 110. Slab #19 extracted rebars condition

Figure 101. Slab #19 after autopsy

***A-T**: Top left bar, **B-T**: Top right bar, **A-B1&B2**: Bottom left bars, **B-B1&B2**: Bottom right bars

b) Rear view

a) Front view

c) Top view

Specimen ID	20A	20B
Top mat	Black	Black
Bar shape (straight/bent)	Straight	Straight
Coating defect (%)	N/A	N/A
Bottom mat		Black
Coating defect (%)	N/A	N/A
Precracked	Yes	Yes

d) Slab specifications

Figure 102. Slab #20 front, rear, and top views with specifications

Figure 103. Slab #20 extracted rebars condition

Figure 104. Slab #20 after autopsy

***A-T**: Top left bar, **B-T**: Top right bar, **A-B1&B2**: Bottom left bars, **B-B1&B2**: Bottom right bars

b) Rear view

a) Front view

c) Top view

Specimen ID	21A	21B
Top mat	Coating D	Coating D
Bar shape (straight/bent)	Straight	Straight
Coating defect (%)	0.5	0.004
Bottom mat	Black	
Coating defect (%)	N/A	N/A
Precracked	Yes	Yes

d) Slab specifications

Figure 105. Slab #21 front, rear, and top views with specifications

96

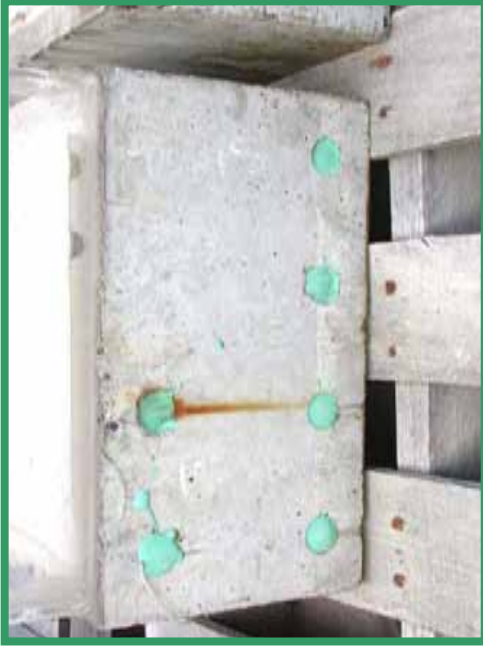Figure 106. Slab #21 extracted rebars condition

Figure 107. Slab #21 after autopsy

***A-T**: Top left bar, **B-T**: Top right bar, **A-B1&B2**: Bottom left bars, **B-B1&B2**: Bottom right bars
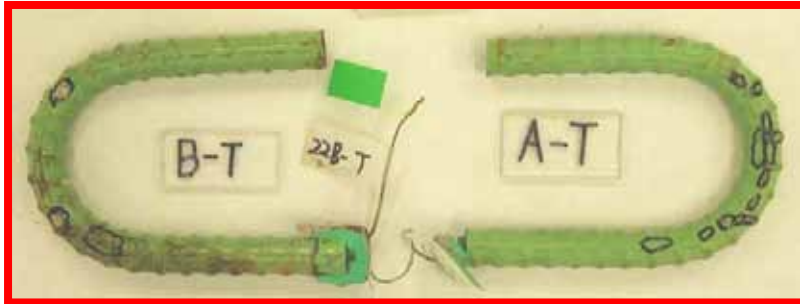
b) Rear view

a) Front view

Specimen ID	22A	22B
Top mat	Coating A	Coating A
Bar shape (straight/bent)	Bent	Bent
Coating defect (%)	0.004	0.5
Bottom mat	Black	
Coating defect (%)	N/A	N/A
Precracked	No	No

d) Slab specifications

c) Top view

Figure 108. Slab #22 front, rear, and top views with specifications
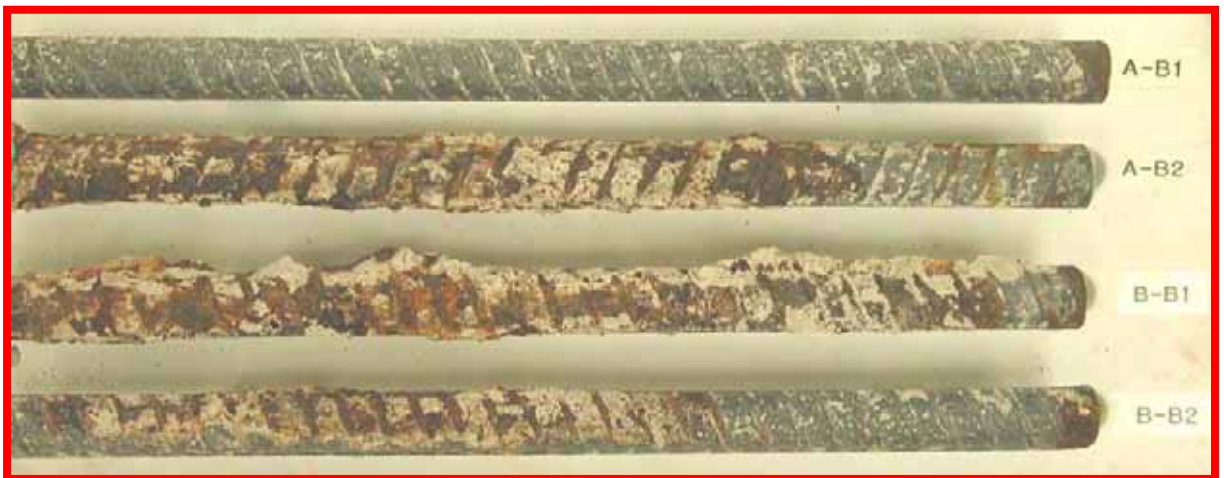
a) Top bars

b) Bottom bars

***A-T**: Top left bar, **B-T**: Top right bar, **A-B1&B2**: Bottom left bars, **B-B1&B2**: Bottom right bars

Figure 109. Slab #22 extracted rebars condition

a) Top bars

b) Bottom bars

***A-T**: Top left bar, **B-T**: Top right bar, **A-B1&B2**: Bottom left bars, **B-B1&B2**: Bottom right bars

Figure 110. Slab #22 after autopsy

b) Rear view

a) Front view

c) Top view

Specimen ID	23A	23B
Top mat	Black	Black
Bar shape (straight/bent)	Bent	Bent
Coating defect (%)	N/A	N/A
Bottom mat		Black
Coating defect (%)	N/A	N/A
Precracked	No	No

d) Slab specifications

Figure 111. Slab #23 front, rear, and top views with specifications

a) Top bars

b) Bottom bars

*__A-T__: Top left bar, __B-T__: Top right bar, __A-B1&B2__: Bottom left bars, __B-B1&B2__: Bottom right bars

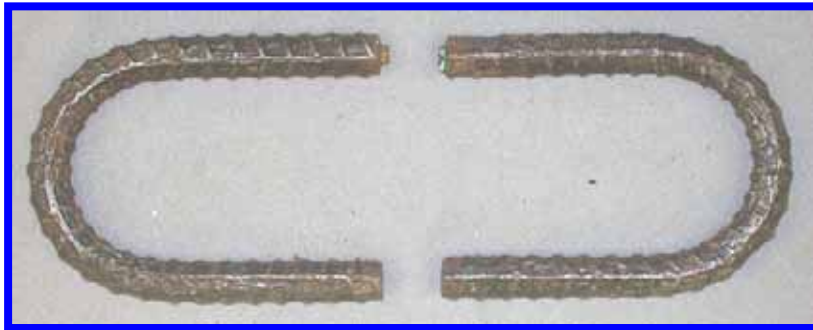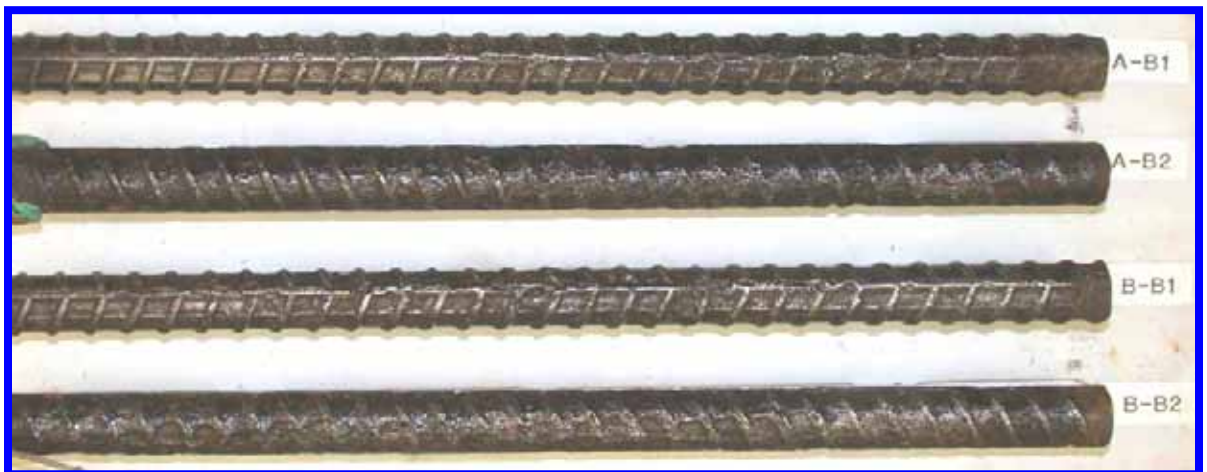Figure 112. Slab #23 extracted rebars condition

a) Top bars

b) Bottom bars

***A-T**: Top left bar, **B-T**: Top right bar, **A-B1&B2**: Bottom left bars, **B-B1&B2**: Bottom right bars

Figure 113. Slab #23 after autopsy

b) Rear view

a) Front view

c) Top view

Specimen ID	24A	24B
Top mat	Coating A	Coating A
Bar shape (straight/bent)	Straight	Straight
Coating defect (%)	0.5	0.004
Bottom mat	Black	
Coating defect (%)	N/A	N/A
Precracked	No	No

d) Slab specifications

Figure 114. Slab #24 front, rear, and top views with specifications

104
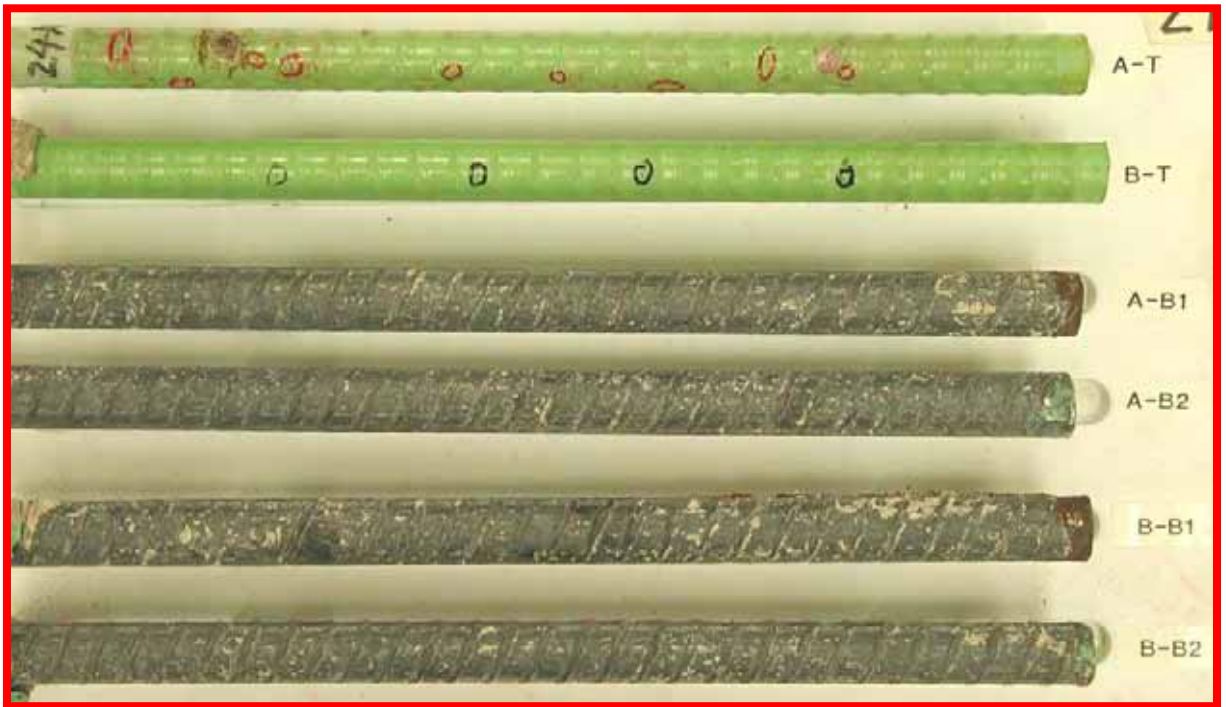
Figure 115. Slab #24 extracted rebars condition

Figure 116. Slab #24 after autopsy

***A-T**: Top left bar, **B-T**: Top right bar, **A-B1&B2**: Bottom left bars, **B-B1&B2**: Bottom right bars

b) Rear view

Specimen ID	25A	25B
Top mat	Coating B	Coating B
Bar shape (straight/bent)	Straight	Straight
Coating defect (%)	0.004	0.5
Bottom mat	Black	
Coating defect (%)	N/A	N/A
Precracked	Yes	Yes

d) Slab specifications

a) Front view

c) Top view

Figure 117. Slab #25 front, rear, and top views with specifications

Figure 118. Slab #25 extracted rebars condition

Figure 119. Slab #25 after autopsy

***A-T**: Top left bar, **B-T**: Top right bar, **A-B1&B2**: Bottom left bars, **B-B1&B2**: Bottom right bars

b) Rear view

a) Front view

c) Top view

Specimen ID	26A	26B
Top mat	Stainless Steel	Stainless Steel
Bar shape (straight/bent)	Straight	Straight
Coating defect (%)	N/A	N/A
Bottom mat	Black	
Coating defect (%)	N/A	N/A
Precracked	No	Yes

d) Slab specifications

Figure 120. Slab #26 front, rear, and top views with specifications

Figure 121. Slab #26 extracted rebars condition

Figure 122. Slab #26 after autopsy

***A-T**: Top left bar, **B-T**: Top right bar, **A-B1&B2**: Bottom left bars, **B-B1&B2**: Bottom right bars

b) Rear view

a) Front view

c) Top view

Specimen ID	27A	27B
Top mat	Stainless Steel	Stainless Steel
Bar shape (straight/bent)	Straight	Straight
Coating defect (%)	N/A	N/A
Bottom mat	Stainless Steel	
Coating defect (%)	N/A	N/A
Precracked	Yes	No

d) Slab specifications

Figure 123. Slab #27 front, rear, and top views with specifications

110

Figure 124. Slab #27 extracted rebars condition

Figure 125. Slab #27 after autopsy

***A-T**: Top left bar, **B-T**: Top right bar, **A-B1&B2**: Bottom left bars, **B-B1&B2**: Bottom right bars

b) Rear view

a) Front view

c) Top view

Specimen ID	28A	28B
Top mat	Coating E	Coating E
Bar shape (straight/bent)	Straight	Straight
Coating defect (%)	0.004	0.5
Bottom mat		Black
Coating defect (%)	N/A	N/A
Precracked	No	No

d) Slab specifications

Figure 126. Slab #28 front, rear, and top views with specifications

112

Figure 127. Slab #28 extracted rebars condition

Figure 128. Slab #28 after autopsy

***A-T**: Top left bar, **B-T**: Top right bar, **A-B1&B2**: Bottom left bars, **B-B1&B2**: Bottom right bars

113

b) Rear view

a) Front view

c) Top view

Specimen ID	29A	29B
Top mat	Coating E	Coating E
Bar shape (straight/bent)	Straight	Straight
Coating defect (%)	0.004	0.5
Bottom mat	Coating E	
Coating defect (%)	0.004	0.5
Precracked	No	No

d) Slab specifications

Figure 129. Slab #29 front, rear, and top views with specifications

114

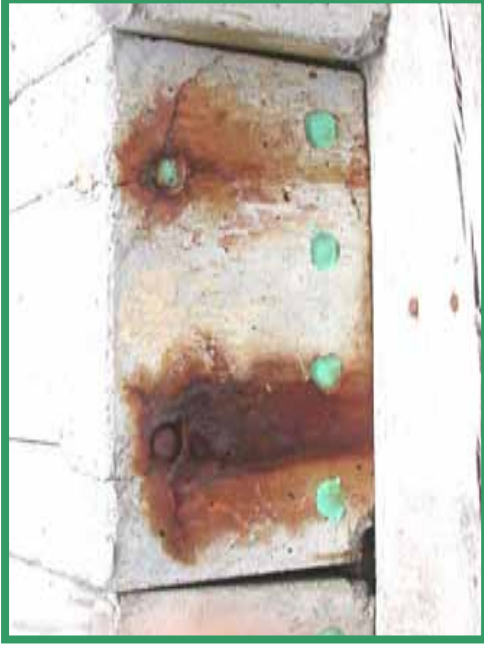Figure 130. Slab #29 extracted rebars condition

Figure 131. Slab #29 after autopsy

***A-T**: Top left bar, **B-T**: Top right bar, **A-B1&B2**: Bottom left bars, **B-B1&B2**: Bottom right bars

b) Rear view

a) Front view

c) Top view

Specimen ID	30A	30B
Top mat	Coating C	Coating C
Bar shape (straight/bent)	Straight	Straight
Coating defect (%)	0.004	0.5
Bottom mat	Black	
Coating defect (%)	N/A	N/A
Precracked	Yes	Yes

d) Slab specifications

Figure 132. Slab #30 front, rear, and top views with specifications

116

Figure 133. Slab #30 extracted rebars condition

Figure 134. Slab #30 after autopsy

***A-T**: Top left bar, **B-T**: Top right bar, **A-B1&B2**: Bottom left bars, **B-B1&B2**: Bottom right bars
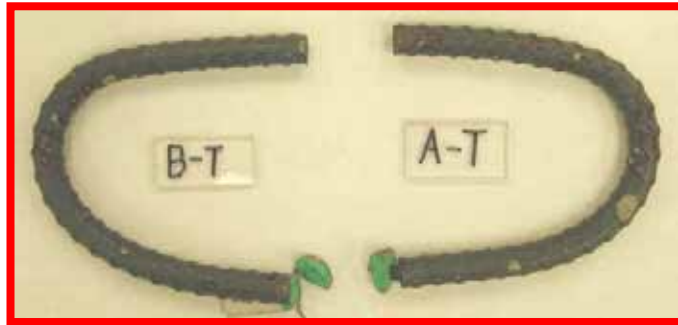
b) Rear view

Specimen ID	31A	31B
Top mat	Coating E	Coating E
Bar shape (straight/bent)	Bent	Bent
Coating defect (%)	0.5	0.004
Bottom mat		Black
Coating defect (%)	N/A	N/A
Precracked	No	No

d) Slab specifications

a) Front view

c) Top view

Figure 135. Slab #31 front, rear, and top views with specifications

118

a) Top bars

b) Bottom bars

***A-T**: Top left bar, **B-T**: Top right bar, **A-B1&B2**: Bottom left bars, **B-B1&B2**: Bottom right bars

Figure 136. Slab #31 extracted rebars condition

a) Top bars

b) Bottom bars

*A-T: Top left bar, **B-T**: Top right bar, **A-B1&B2**: Bottom left bars, **B-B1&B2**: Bottom right bars

Figure 137. Slab #31 after autopsy